UNIVERSIDAD DE CHILE
FACULTAD DE CIENCIAS FíSICAS Y MATEMÁTICAS
DEPARTAMENTO DE FÍSICA

ELECTRON LOCALIZATION IN INTRAMOLECULAR PROTON TRANSFER

TESIS PARA OPTAR AL GRADO DE
MAGÍSTER EN CIENCIAS, MENCIÓN FÍSICA

BORIS EDUARDO MAULÉN JARA

PROFESOR GUÍA :
CARLOS CÁRDENAS VALENCIA
PROFESOR GUÍA 2:
PATRICIO FUENTEALBA ROSAS

MIEMBROS DE LA COMISIÓN:
ÁLVARO NÚÑEZ VÁSQUEZ
TATIANA GÓMEZ CANO
LUIS FOA TORRES

SANTIAGO DE CHILE
2019

RESUMEN DE LA MEMORIA PARA OPTAR
AL TÍTULO DE MAGÍSTER EN CIENCIAS, MENCIÓN FÍSICA
POR: BORIS EDUARDO MAULÉN JARA
FECHA: 2019
PROF. GUÍA: CARLOS CÁRDENAS VALENCIA PATRICIO FUENTEALBA ROSAS

ELECTRON LOCALIZATION IN INTRAMOLECULAR PROTON TRANSFER

The electron localization function (ELF) is a scalar field that accounts of the excess of electronic kinetic energy due to Pauli repulsion between electrons with the same spin. With this function, it is possible to divide real space in regions (basins) where electronic localization is high and Pauli repulsion is low (up-down electron pairs). From a phenomenological point of view, bifurcation points of the localization domains (points that belong to certain basins of a molecule) can be used to describe the rupture and formation of chemical bonds. Moreover, topological analysis of ELF allows us performing a statistical analysis of the electronic population of basins in a molecule. In this work, by using density functional theory with an hybrid exchange-correlation functional, we describe the electron localization along the intramolecular proton transfer in the Salicidene Methilamine molecule (SMA). First we do it in the ground state, in order to acquire physical insight of the process. Later, by means of time-dependent density functional theory (TD-DFT) in the linear response regime, we perform an equivalent analysis in the first excited state, for which we propose a way to compute ELF in excited states using TD-DFT. We show how the electronic population and other properties of interest of the basins associated with the atoms and bonds involved in the proton transfer change during the reaction. Finally, we choose this system because, after photoexcitation and proton transfer process, SMA suffers a large Stokes shift followed by a "closed" photocycle that ends with the molecule in its original ground state. This makes molecules like SMA good prospects for molecular photoswitches. The main contribution of this thesis is that this is the first time that the ELF developed and successfully used to explain chemical bonding in excited states.

Resumen

LOCALIZACIÓN ELECTRÓNICA EN LA TRANSFERENCIA PROTÓNICA INTRAMOLECULAR

La función de localización electrónica (ELF) es un campo escalar que da cuenta del exceso de energía cinética electrónica debido a la repulsión de Pauli entre electrones con igual spin. Con esta función, es posible dividir el espacio real en regiones (cuencas) donde la localización electrónica es grande y la repulsión de Pauli es baja (pares de electrones up-down). Desde un punto de vista fenomenológico, los puntos de bifurcación de los dominios de localización (puntos que pertenecen a ciertas cuencas de la molécula) pueden ser usados para describir la ruptura y formación de enlaces químicos. Más aún, el análisis topológico de la ELF nos permite realizar un análisis estadístico de las poblaciones electrónicas de las cuencas en una molécula. En este trabajo, usando teoría del funcional de la densidad con un funcional de correlación-intercambio híbrido, describimos la función de localización electrónica a lo largo de la transferencia protónica intramolecular en la molécula de Saliciden Metilamina (SMA). Primero hicimos ésto en el estado fundamental, a fin de adquirir una visión física del proceso. Luego, por medio de teoría del funcional de la densidad dependiente del tiempo (TD-DFT) en el regimen de respuesta lineal, realizamos un análisis equivalente en el primer estado excitado, para el cual proponemos una forma de calcular la ELF en estados excitados usando TD-DFT. Mostramos cómo la población electrónica y otras propiedades de interés de las cuencas asociadas con los enlaces y los átomos involucrados en la transferencia protónica cambian durante la reacción. Finalmente, hemos escogido este sistema ya que, tras la fotoexcitación y la transferencia protónica, la molécula de SMA sufre un gran *Stokes shift* seguido de un fotociclo "cerrado" el cual termina con la molécula en su estado fundamental original. Esto hace a moléculas como la SMA buenos prospectos para *fotoswitches* moleculares. La principal contribución de esta tesis es que ésta es la primera vez que la ELF es desarrollada y satisfactoriamente usada para explicar enlaces químicos en estados excitados.

A Carmen

Al viento, las montañas, a los tímidos amaneceres y al ocaso anaranjado de principios de verano.

A John Coltrane por su exquisita balada "Naima", y a Bruno Limbardo por su silente y oscura compañía.

"Nunca llegaré a ser un poeta; sólo me parecen bellas unas pocas cosas obvias: ..., tardes de primavera, música de noche, el mar; no soy capaz de comprender cosas más sutiles como «las trompetas que tocan a plata». Podré llegar a ser un intelectual pero nunca escribiré más que poesía mediocre"

A este lado del paraíso, ***F. Scott Fitzgerald***

Agradecimientos

A el Proyecto Basal CEDENNA FB0807 y a el Proyecto Fondecyt 1181121. Al Departamento de Física (dfi) de la Facultad de Ciencias Físicas y Matemáticas y al Departamento de Física (DFC) de la Facultad de Ciencias, sendas instituciones de física de la Universidad de Chile. A mis compañeros del diverso e interdisciplinario grupo de Física Química Teórica del DFC de la Universidad de Chile. A Carmen Nabalón por su constante asesoría profesional en la redacción de esta tesis, y por sobre todo, por su apoyo en las decisiones que he debido tomar tanto en el plano académico como en lo personal.

Contents

List of Tables

List of Figures

Chapter 1

Introduction

1.1 Physical description of chemical bond

"*Chemistry has its own concepts, its own level of understanding which explains the properties of the matter from its composition in terms of elements and of their position in the periodic table rather from physical laws mastered by Schrödinger equation*"

Linus Pauling

The description of the chemical bond from a physical point is not unique, but, in general, relies on quantum mechanics. A covalent chemical bond can be seen as formed by a pair of electrons of opposite spin, usually located between two atoms, which impose structural stability to molecules. Also, electrons are fermions, and hence, its field operators $a_i(\mathbf{r})$ and $a_i^\dagger(\mathbf{r})$ fulfills the Grassmann algebra,

$$\left\{a_i(\mathbf{r}), a_j^\dagger(\mathbf{r}')\right\} = \delta^3(\mathbf{r}-\mathbf{r}')\delta_{ij}, \qquad \{a(\mathbf{r}), a(\mathbf{r}')\} = \left\{a^\dagger(\mathbf{r}), a^\dagger(\mathbf{r}')\right\} = 0, \tag{1.1}$$

where the Pauli exclusion principle, which is a consequence of the antisymmetry of fermionic states, is encoded in the second anticommutator.

On the other hand, in analogy to a classical system, it is possible to describe the chemical bond by a quantum harmonic oscillator where energy eigenvalues correspond to the energy of vibration of the bond. However, a harmonic oscillator has only discrete spectra and can not describe the rupture or the formation of chemical bonds. This approach can be improved replacing the harmonic oscillator for an anharmonic one. The advantage of this last kind of oscillator is that it contains both discrete and continuum spectra, and thus, allows us to calculate bound to continuum probability transitions, which are responsible for the rupture of bonds [36]. Thus, within this approach, the knowledge of the chemical bond it is reduced to solve of the corresponding Schrödinger equation for a particular internuclear potential function. In diatomic molecules, there are many works in this direction, which use different resolution techniques of the molecular Schrödinger equation, namely, via hypergeometric series, numerical methods or, in the exceptional case when this equation has an

analytical solution, via Lie algebras [37]-[38]-[39]-[40]. Unfortunately, as long as the number of electrons in the molecule increases, the complexity of the Schrödinger equation becomes overwhelming, due to the interelectronic repulsion between all electrons and the large number of variables that the wave function depends on (for a N electron system, the wave function depends on $3N$ spatial coordinates and N spin coordinates). Hence, it is important to count with an approach that allows describing the physics of the chemical bond without solving a formidable differential equation. In this sense, density functional theory (DFT) solve the problem. DFT is a quantum-statistical approach to many-particle (fermion) systems, which have as a fundamental variable the electronic density $\rho(\mathbf{r})$, that corresponds to the coordinate representation of the diagonal element of the first-order reduced density matrix of a pure many-particle state $|\Psi\rangle$. Note that all molecular systems have a Hamiltonian with the same form, differing only in the number of electrons, N, and the external potential, $v(\mathbf{r})$, that is, the Coulomb attraction that nuclei exert on the electrons. Then, the many-particle ground state of the molecule depends on these two quantities and so does any observable. The essential statement of DFT is that $\rho(\mathbf{r})$, instead of N and $v(\mathbf{r})$, can be used as a basic variable, by means of which all molecular observables are functional. This statement is formalized in the first *Hohenberg and Kohn* theorem, which states that there is an isomorphism between the space of the external potentials $v(\mathbf{r})$ and the space of all *v-representable* electron densities, so that there are no two different external potentials that give the same $\rho(\mathbf{r})$ [28]. The first example of the functional dependence on $\rho(\mathbf{r})$ appears in quantum statistical mechanics, in the problem of the non-relativistic non-interacting Fermi gas of electrons, whose total kinetic energy is given by [42]

$$T[\rho] = \frac{3\hbar^2}{5m_{\mathrm{e}}}\left(\frac{9\pi^4}{2}\right)^{1/3}\int \rho(\mathbf{r})^{5/3}\mathrm{d}\mathbf{r}. \tag{1.2}$$

The second *Hohenberg and Kohn* theorem provides to the theory a variational structure. Thereby, the total energy and the electron density are obtained by solving a Euler-Lagrange equation, avoiding thus to solve the corresponding Schrödinger equation. Many concepts used by chemist which, in general, have an important empirical component, can be described by DFT. Concepts associated with chemical reactivity find a physical definition in DFT, for instance, the chemical potential, μ, is defined as [27]

$$\mu = \frac{\delta E[\rho]}{\delta \rho} = \left(\frac{\partial E}{\partial N}\right)_v. \tag{1.3}$$

In general, most chemical concepts belong to the real space. Then, if we are interested in describing the chemical bond using quantum mechanics, we should find a way of mapping the objects of a fermionic Fock space into objects that lie in $\mathbb{R}^3$. The *Electron Localization Function* (ELF) partitions the real space in regions associated with electron pairs by measuring their spatial localization. The ELF arises from the local behavior of the Hartree-Fock exchange density and accounts for the probability of finding two electrons of the same spin around a given point of $\mathbb{R}^3$ [1]. Thereby, with the ELF it is possible to divide real space into regions (basins) where electronic localization is high, and Pauli repulsion is low. These regions can be either non-bonding electron pairs, internal core electrons shells or chemical bonds [2].

1.2 Intramolecular proton transfer

Although many chemical reactions occur in the ground state, many others occur in electronically excited states. Molecules reach excited states through the absorption of radiation. Photophysics and photochemistry study the physics of the excitation and deexcitation mechanism and the molecular changes (reactions) that these processes entail. Examples of processes that occur after absorption of radiation are photodissociation, geometric isomerization, and tautomerization. Of particular importance is the *excited state intramolecular proton transfer* (ESIPT) [18]-[24]. In general, an intramolecular hydrogen bond (H-bond) between an acid group (with a tendency to give a proton) and a basic group (with a tendency to accept it) is a signature of molecules with ESIPT. A prototypal molecule with ESIPT is the *salicidene methylamine* (SMA) [19]-[23]-[26]. The molecular structure of SMA is shown in Figure 1.1. In this representation, spheres represent atoms: gray are carbons, white hydrogens, red is oxygen and blue is nitrogen. Sticks represent chemical bonds: a single stick is a simple bond, a double stick is a double bond, and a dashed one represent electronic delocalization along the six-carbon ring. In particular, in SMA molecule, the donor group is the *hydroxyl* (OH), while the acceptor is the nitrogen atom (N).

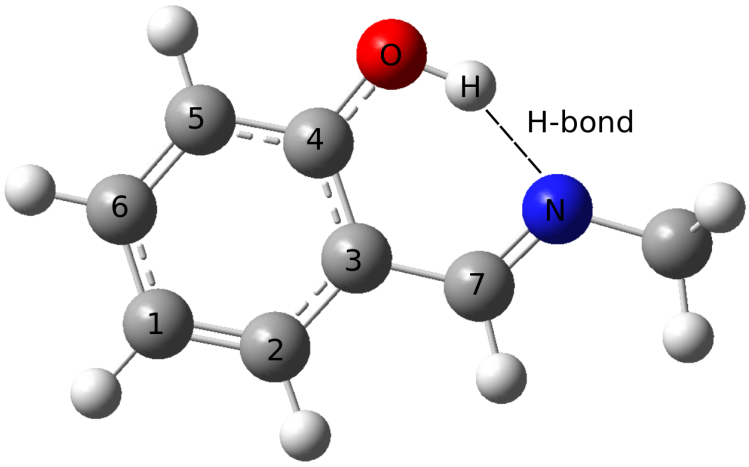

Figure 1.1: SMA molecule.

The barrier for the proton transfer in the ground state of SMA (S_0) is several orders of magnitude higher than thermal energy and, therefore, the process is not observed at room temperature and pressure. After absorption of radiation, the molecule is excited to its first singlet excited state (S_1) in which the proton transfer occurs without an energy barrier. This process, called *Enol* $\rightarrow$ *Keto* tautomerism is accompanied by a displacement of the maximum absorption wavelength to a higher wavelength (*Stokes shift*). Therefore, the radiation emitted by fluorescence by the Keto form is of lower frequency than the radiation that absorbed the Enol form. This phenomenon is called *photochromism*. On the other hand, after the ESIPT process, the molecule can undergo a geometrical isomerization, that is, a rotation of the bond $C3 - C7$ (see Figure 1.2), which allows the system to return to the ground state, in a non-radiative way, through a conical intersection (**CI** in the Figure 1.2). The decay to the ground state by emission of radiation can lead to the molecule to its original (Enol) form through a proton transfer in S_0 (GSIPT). There may also be a considerable fraction of molecules trapped in the keto form. It is this photochemical cycle between both, Enol and Keto forms, that makes this kind of compounds good prospects for molecular photoswitches [22].

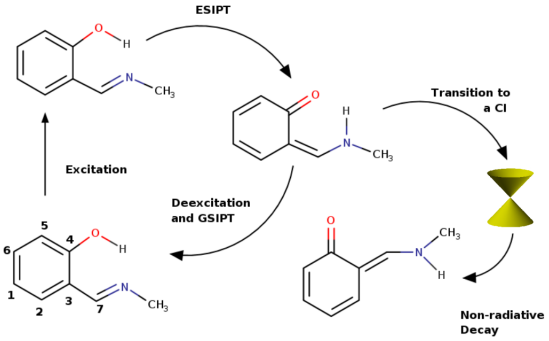

Figure 1.2: Photochemical and photophysical process in the SMA molecule

In order to get a physical insight of the ESIPT process, we have performed ground state calculations on the SMA. As a first approximation, we can consider the displacement of the hydrogen atom from the oxygen to the nitrogen as the path that follows the process. Then, for a given $(O-H)$ distance, the position of remaining atoms are relaxed until the force of them is zero. This type of procedure is known in quantum chemistry as *relaxed scan* calculation, and its purpose is to evaluate the change of the molecular energy with the change of some structural degree of freedom [35]. The resulting potential energy surface (PES), with the zero set to the energy of the initial molecular geometry (Enol), has a maximum at the internuclear distance $r_{O-H} = 1.28$Å, with an energetic barrier of $0.31eV$ $(28.8kJ/mol)$. The maximum point of the PES is called *transition state* (TS), and for a chemical reaction occurs, the molecule must overcome this barrier.

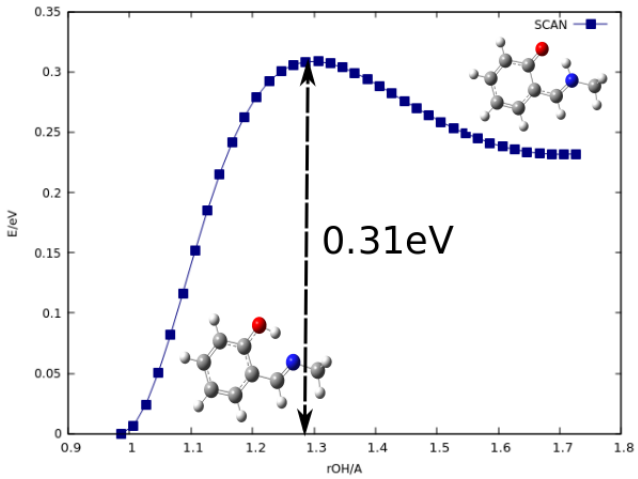

Figure 1.3: Relaxed scan along oxygen-hydrogen internuclear distance in the ground state.

Chapter 2

Electron localization function

2.1 Electron localization function in the Hartree-Fock approximation

In the Hartree-Fock (HF) approximation, a quantum state of an N-electrons system is given by

$$|\Psi_N\rangle = \frac{1}{\sqrt{N!}} \sum_p (-1)^p \, |\psi_{p1}\rangle \otimes ... \otimes |\psi_{pN}\rangle \,, \tag{2.1}$$

which is a Slater determinant of one-particle basis kets (HF spin-orbitals) $\{|\psi_{\mathrm{i}}\rangle\}$. These orbitals constitute a mean-field solution. Similarly, the density matrix of a pure state of N electrons, $\hat{\gamma}_N \doteq |\Psi_N\rangle \langle\Psi_N|$, has a space representation given by

$$\gamma_N(\mathbf{x}'_1, ..., \mathbf{x}'_N; \mathbf{x}_1, ..., \mathbf{x}_N) = \langle \mathbf{x}'_1, ...| \, \hat{\gamma}_N \, |\mathbf{x}_1, ...\rangle \,, \tag{2.2}$$

where $\mathbf{x}_{\mathrm{i}} \doteq (\mathbf{r}_{\mathrm{i}}, \sigma)$ includes both spatial ($\mathbf{r}$) and spin (σ) coordinates. To calculate statistical averages of molecular properties, we need to work with reduced density matricies (RDM), which are defined as

$$\gamma_s(\mathbf{x}'_1, ..., \mathbf{x}'_s; \mathbf{x}_1, ..., \mathbf{x}_s) \doteq \binom{N}{s} \int \mathrm{d}\mathbf{x}_{s+1} ... \mathrm{d}\mathbf{x}_N \gamma_N(\mathbf{x}'_1, ..., \mathbf{x}'_s, \mathbf{x}_{s+1}, ..., \mathbf{x}_N; \mathbf{x}_1, ..., \mathbf{x}_s, \mathbf{x}_{s+1}, ..., \mathbf{x}_N), \tag{2.3}$$

where s is the order of the reduced density matrix. Expressions for second and first-order RDM are

$$\gamma_2(\mathbf{x}'_1, \mathbf{x}'_2; \mathbf{x}_1, \mathbf{x}_2) = \binom{N}{2} \int \mathrm{d}\mathbf{x}_3 ... \mathrm{d}\mathbf{x}_N \gamma_N(\mathbf{x}'_1, \mathbf{x}'_2 ...; \mathbf{x}_1, \mathbf{x}_2, ...), \tag{2.4}$$

and

$$\gamma_1(\mathbf{x}'_1, \mathbf{x}_1) = N \int \mathrm{d}\mathbf{x}_2 ... \mathrm{d}\mathbf{x}_N \gamma_N(\mathbf{x}'_1, \mathbf{x}_2, ...; \mathbf{x}'_1, \mathbf{x}_2, ...). \tag{2.5}$$

Now, in abscence of external magnetic fields, the molecular Hamiltonian in the coordinate representation is given by,

$$\hat{H}_N = \sum_{\mathrm{i}=1}^{N} \left(-\frac{1}{2}\nabla_{\mathrm{i}}^2 + v(\mathbf{r}_{\mathrm{i}}) \right) + \frac{1}{2} \sum_{\mathrm{i}=1}^{N} \sum_{j \neq \mathrm{i}}^{N} \frac{1}{r_{\mathrm{i}j}}, \tag{2.6}$$

where the first term corresponds to a sum of one-particle Hamiltonians $\hat{h}_{\mathrm{i}} = -\frac{1}{2}\nabla_{\mathrm{i}}^2 + v(\mathbf{r}_{\mathrm{i}})$, with

$$v(\mathbf{r}_{\mathrm{i}}) = -\sum_{\alpha=1}^{M} \frac{Z_\alpha}{r_{\mathrm{i}\alpha}} \tag{2.7}$$

the external field exerted by the M nuclei of the molecule on the i-*th* electron. Note that in the molecular Hamiltonian there is not spin dependence. Hence, we can trace out the spin coordinates in (2.4) and (2.5), to obtain the spinless RDM,

$$\rho_2(\mathbf{r}_1', \mathbf{r}_2'; \mathbf{r}_1, \mathbf{r}_2) = \binom{N}{2} \sum_{\sigma_1, \sigma_2'} \int \mathrm{d}\mathbf{x}_3 ... \gamma_N((\mathbf{r}_1', \sigma_1), (\mathbf{r}_2', \sigma_2') ...; (\mathbf{r}_1, \sigma_1), (\mathbf{r}_2, \sigma_2') ...), \tag{2.8}$$

and

$$\rho_1(\mathbf{r}_1', \mathbf{r}_1) = N \sum_{\sigma} \int \mathrm{d}\mathbf{x}_2 ... \mathrm{d}\mathbf{x}_N \gamma_N((\mathbf{r}_1', \sigma), \mathbf{x}_2, ...; (\mathbf{r}_1, \sigma), \mathbf{x}_2, ...). \tag{2.9}$$

Furthermore, the total molecular energy is expressed as a functional of the spinless reduced density matrices (2.8) and (2.9) as follows:

$$E\left[\rho_1, \rho_2\right] = \int \mathrm{d}\mathbf{r} \left(-\frac{1}{2}\nabla_{\mathbf{r}}^2 + v(\mathbf{r}) \right) \rho_1(\mathbf{r}', \mathbf{r}) \Big|_{\mathbf{r}=\mathbf{r}'} + \int \mathrm{d}\mathbf{r}_1 \mathrm{d}\mathbf{r}_2 \frac{\rho_2(\mathbf{r}_1', \mathbf{r}_2'; \mathbf{r}_1, \mathbf{r}_2)}{|\mathbf{r}_2 - \mathbf{r}_1|} \Big|_{\mathbf{r}_1=\mathbf{r}_1'; \mathbf{r}_2=\mathbf{r}_2'}. \tag{2.10}$$

A consequence of the approximate nature of the Hartree-Fock wavefunction is that high order RDM can be written in terms of RDMs of a lower order. Thus, γ_2 in terms of γ_1 is [28]

$$\gamma_2(\mathbf{x}_1', \mathbf{x}_2'; \mathbf{x}_1, \mathbf{x}_2) = \frac{1}{2} \begin{vmatrix} \gamma_1(\mathbf{x}_1', \mathbf{x}_1) & \gamma_1(\mathbf{x}_2', \mathbf{x}_1) \\ \gamma_1(\mathbf{x}_1', \mathbf{x}_2) & \gamma_1(\mathbf{x}_2', \mathbf{x}_2) \end{vmatrix}, \tag{2.11}$$

where γ_1 has a spectral decomposition in terms of the HF spin-orbitals,

$$\gamma_1(\mathbf{x}_1', \mathbf{x}_1) = \sum_{\mathrm{i}}^{N} \psi_{\mathrm{i},\sigma}(\mathbf{x}_1') \psi_{\mathrm{i},\sigma}^*(\mathbf{x}_1), \tag{2.12}$$

called the first-order *Fock-Dirac reduced density matrix.*

Also, it is possible to obtain a simple expression for ρ_2 using (2.11), and considering that the exchange (given by the off-diagonal elements of the determinant) is different from zero only for components of the density of the same spin. Hence, ρ_2 in terms of its spin $|+\rangle$ and $|-\rangle$ components is given by

$$\rho_2(\mathbf{r}_1, \mathbf{r}_2; \mathbf{r}_1, \mathbf{r}_2) \doteq \rho_2(\mathbf{r}_1, \mathbf{r}_2) = \rho_2^{|+\rangle|+\rangle}(\mathbf{r}_1, \mathbf{r}_2) + \rho_2^{|-\rangle|-\rangle}(\mathbf{r}_1, \mathbf{r}_2) + \rho_2^{|+\rangle|-\rangle}(\mathbf{r}_1, \mathbf{r}_2) + \rho_2^{|-\rangle|+\rangle}(\mathbf{r}_1, \mathbf{r}_2), \tag{2.13}$$

where each term means

$$\rho_2^{|\sigma\rangle|\sigma'\rangle}(\mathbf{r}_1,\mathbf{r}_2) \doteq \gamma_2(\mathbf{r}_1,|\sigma\rangle\,;\mathbf{r}_2,|\sigma'\rangle). \tag{2.14}$$

Now, using (2.11) for each of the four components in (2.13), one obtains

$$\rho_2(\mathbf{r}_1,\mathbf{r}_2) = \frac{1}{2}\rho(\mathbf{r}_1)\rho(\mathbf{r}_2) - \frac{1}{4}|\rho_1(\mathbf{r}_1,\mathbf{r}_2)|^2. \tag{2.15}$$

From the above equation is easy to understand the physical meaning of the spinless second-order RDM. This is a pair probability density, where the first term corresponds to a uncorrelated statistical product between the electronic densities of any two electrons, while the second term is due to the exchange correlation between them. This exchange correlation is a manifestation of the Pauli's exclusion principle. Then, the conditional probability of finding an electron located in $\mathbf{r}_2$ separated a distance $s \doteq |\mathbf{r}_2 - \mathbf{r}_1|$ of a electron located in a reference point $\mathbf{r}_1$ is given simply by

$$P(\mathbf{r}_2|\mathbf{r}_1) = \frac{\rho_2(\mathbf{r}_1,\mathbf{r}_2)}{\rho(\mathbf{r}_1)} = \frac{1}{2}\rho(\mathbf{r}_2) + \frac{1}{2}\rho_x(\mathbf{r}_1,\mathbf{r}_2), \tag{2.16}$$

where

$$\rho_x(\mathbf{r}_1,\mathbf{r}_2) = -\frac{1}{2}\frac{|\rho_1(\mathbf{r}_1,\mathbf{r}_2)|^2}{\rho(\mathbf{r}_1)} = -h_x(\mathbf{r}_1,\mathbf{r}_2) \tag{2.17}$$

is the exchange density (the negative of the exchange hole $h_x(\mathbf{r}_1,\mathbf{r}_2)$). Thus, in order to focus on the Pauli repulsion between electrons, we define the conditional pair probability of the same spin $P(\mathbf{r}_2,\sigma|\mathbf{r}_1,\sigma)$ as

$$P(\mathbf{r}_2,\sigma|\mathbf{r}_1,\sigma) \doteq \frac{\rho_{2\sigma}(\mathbf{r}_1,\mathbf{r}_2)}{\rho_\sigma(\mathbf{r}_1)} \tag{2.18}$$

$$= \rho_\sigma(\mathbf{r}_2) - \frac{|\rho_1^\sigma(\mathbf{r}_1,\mathbf{r}_2)|^2}{\rho_\sigma(\mathbf{r}_1)}, \tag{2.19}$$

where $\rho_{2\sigma}$ corresponds to the sum of second-order RDMs with parallel spin, i.e.,

$$\rho_{2\sigma} \doteq \rho_2^{|\sigma\rangle|\sigma\rangle} = \rho_2^{|+\rangle|+\rangle} + \rho_2^{|-\rangle|-\rangle}. \tag{2.20}$$

Becke showed that the spherical average of $P(\mathbf{r}_2,\sigma|\mathbf{r}_1,\sigma)$ around a middle point between electrons is, up to second order in the distance between electrons, s, given by [2]

$$\begin{aligned}\langle P(\mathbf{r}_2,\sigma|\mathbf{r}_1,\sigma)\rangle &= \frac{s^2}{3!}\nabla_{\mathbf{s}}^2 P(\mathbf{r}_2,\sigma|\mathbf{r}_1,\sigma)\Big|_{\mathbf{r}_1=\mathbf{r}_2} + O(s^4),\\ &= \frac{s^2}{3}\left[\sum_{i=1}^{N/2}|\nabla_{\mathbf{r}}\psi_{i,\sigma}(\mathbf{r})|^2 - \frac{|\nabla_{\mathbf{r}}\rho_\sigma(\mathbf{r})|^2}{\rho_\sigma(\mathbf{r})}\right],\\ &= \frac{s^2}{3}D_\sigma(\mathbf{r}),\end{aligned} \tag{2.21}$$

with

$$D_\sigma(\mathbf{r}) = \frac{1}{2}\nabla_{\mathbf{r}}^2 P(\mathbf{r}_2,\sigma|\mathbf{r}_1,\sigma)\Big|_{\mathbf{r}_1=\mathbf{r}_2} \tag{2.22}$$

a scalar field proportional to the curvature of the conditional pair probability, which measures the excess of kinetic energy density of the electrons consequence of its fermionic nature, and hence is called *delocalization field*. The first term in the square bracket of Eq. (2.21) is the kinetic energy density of electrons, which is a functional of the occupied HF spin-orbitals, while the second term is the same quantity for a bosonic system of equal density as the fermionic system. This term it is known as the von Weizsäcker kinetic energy density. Also, from $D_\sigma(\mathbf{r})$ it is possible to define the *Electron localization function* (ELF), which is a Lorentzian normalization of $D_\sigma(\mathbf{r})$,

$$\eta(\mathbf{r}) = \frac{1}{1 + \left(\frac{D_\sigma(\mathbf{r})}{D_\sigma^0}\right)^2}. \tag{2.23}$$

$\eta(\mathbf{r})$ is a measure of electronic localization and allows us to identify regions of the space where the probability of finding two neighboring electrons of the same spin is low. D_σ^0 in (2.23) is the kinetic energy of the non-interacting Fermi gas (Eq. (1.2)). Thus, ELF is close to its maximum value (1) in regions where electrons are poorly correlated, that is, where the second-order RDM is basically given by an uncorrelated product of electronic densities. An alterantive interpretation given by Savin is that in regions of large ELF, the Pauli's principle imposes a small excess of kinetic energy to electrons, approaching to a bosonic behaviour [4]. In a molecule, these regions usually correspond to chemical bonds or non-bonding electron pairs (in both cases, these regions are conformed by up-down electron pairs). On the other hand, ELF tends to 0 in regions of maximum delocalization, that is, in regions where electrons strongly fluctuate because their kinetic energy is large.

2.2 Elements of catastrophe theory

A chemical reaction is a dynamical process in which, upon variation of nuclear coordinates, chemical bonds break and form, leading to new molecules. Hence, nuclear coordinates corresponds to *control parameters* which defines the *control space*. To describe a chemical process as a dynamical system is necessary to introduce certain concepts from topology, which will allow us to study topological changes when control parameters are varied. These concepts belong to the *Tom's Catastrophe theory*.

A dynamical system is defined by

$$\dot{x}_i(c_\alpha; t) = f_i(x_i; c_\alpha; t), \tag{2.24}$$

where $\mathbf{x}$ are the trajectories defined in the manifold M of internal states, c_α are the control parameters, and f_i can be understood as a component of a velocity field. Note that (2.24) defines an equation of motion in the space of trajectories. If $\mathbf{f}$ is time-independent, it can be written as a gradient of a scalar field (potential function) $V(\mathbf{x}; c_\alpha)$. In this case, the dynamical system is called *gradient dynamical system*, and is defined by

$$\dot{x}_i(c_\alpha; t) = \frac{\partial V(x_j; c_\alpha)}{\partial x_i}. \tag{2.25}$$

All trajectories begin and end at equilibrium points, that is, points where $\dot{x}_i(c_\alpha; t) = 0$. These points are called *critical points*, and, for a gradient dynamical system, are defined by

$$\frac{\partial V(x_j; c_\alpha)}{\partial x_i} = 0. \tag{2.26}$$

Also, critial points $\mathbf{x}_c$ are characterized by an index $I(\mathbf{x}_c)$ called *critical exponent*, which corresponds to the number of positive eigenvalues of the Hessian matrix H_{ij} of the potential function $V(\mathbf{x}; c_\alpha)$, that is

$$H_{ij}(\mathbf{x}_c) = \left.\frac{\partial^2 V(\mathbf{x}; c_\alpha)}{\partial x_i \partial x_j}\right|_{\mathbf{x}=\mathbf{x}_c} \tag{2.27}$$

Thus, for $I = 3$, a critial point is a local minimum and is called a *repellor*. $I = 1, 2$ correspond to saddle points, and finally $I = 0$ defines a local maximum and is called an *attractor*. Now, considering an arbitrary point $\mathbf{x}_0$ and taking the limit $t \to \infty$, the point $\mathbf{x}_p$ to which the trajectory starting in $\mathbf{x}_0$ converges, is called the *ω-limit*. An *ω-limit* is also an attractor. The set of points that converge to the same attractor is called the *basin* of this attractor, and it defines its domain of structural stability [8]-[9].

In the language of the *bonding evolution theory* [7], the trajectories $\mathbf{x}$ are points in $\mathbb{R}^3$ and the control parameters $\{c_\alpha\}$ are the nuclear coordinates $\{\mathbf{R}_\alpha\}$. The potential function,$V(\mathbf{x}; c_\alpha)$, has to be a field with information on bond regions; in this case the ELF. A great advantage of using the ELF to describe the electronic structure of molecules is that it allows dividing the molecular space into different regions according to how localized the electrons are. These regions, $\{\Omega_i\}$, of high electronic localization, are the basins defined above, and they correlate well with the regions associated with chemical bonds and lone pairs [4]. Basins of ELF are classified according to the number of atomic cores that are involved (synaptic order), and whether they enclose atomic cores or valence electrons. For example, $C(A)$ is a monosynaptic basin associated with the core of the atom A, $V(A)$ is a monosynaptic basin related to the valence structure of the atom A, $V(A, B)$ is a disynaptic basin related to the valence structure shared by the two atoms A and B, and so forth [11]. Valence monosynaptic basins correspond to non-bonding electron pairs located around atomic centers, and valence disynaptic basins are associated with chemical bonds. Basins associated with atomic cores are only monosynaptic. The attractors of ELF basins may or not coincide with atomic centers. Thus, only attractors of core basins coincide with atomic positions, while attractors of valence monosynaptic basins are located around an atomic core but separated from it a certain distance. Disynaptic valence attractors are located between two or more atoms involved in a chemical bond.

Through critical points, $\mathbf{r}_c$, where the gradient of ELF vanishes,

$$\nabla_{\mathbf{r}} \eta(\mathbf{r}_c; \mathbf{R}^*) = 0, \tag{2.28}$$

one identifies *bifurcation points* between adjacent basins, which, in turn, define the *localization domains*. Specifically, for a certain nuclear configuration of the molecule, $\mathbf{R}^*$, bifurcation points are critical points where the determinant of Hessian matrix $H_{ij} \doteq \partial^2\eta/\partial x_i \partial x_j$ vanishes,

$$\left.\det\left(\frac{\partial^2 \eta}{\partial x_i \partial x_j}; \mathbf{R}^*\right)\right|_{\mathbf{r}_c} = 0. \tag{2.29}$$

Moreover, bifurcation points give us a qualitative measure about the electronic delocalization between two basins: the smaller the ELF in a bifurcation point between two adjacent basins, the lower the delocalization between them (electrons are more localized in their respective basins). The contrary also applies, bifurcation points with high values of ELF indicate large electronic fluctuation between the basins. A localization domain is a domain of structural stability of certain attractors, and it corresponds to a certain region of the space enclosed by some value of the ELF, i.e., it could be a subsets of basins [8]. Localization domains may be *reducible* or *irreducible*. A localization domain is *reducible* if there is a value of ELF at which the volume that defines the domain splits in two or more basins corresponding to simpler domains. This process corresponds to a reduction of localization and occurs at a critical point with critical exponent 1 (saddle point) located on the boundary of the basins involved. An irreducible domain is one that cannot be reduced by bifurcation points and enclose only one attractor.

Finally, with the concepts defined above, a chemical reaction can be understood as a transition from one structural stability domain, or bonding state, to another through *bifurcation catastrophes*, i.e., through points in the reaction path at which are changes in the synaptic order of the basins [8].

2.2.1 Core-valence bifurcation index

The choice of the ELF as a function for monitoring a chemical process, instead of the electron density, is done because the ELF provides a clear differentiation between covalent and some non-covalent interactions. In this sense, it is possible to answer the question if a hydrogen-bonded complex represents a unitary molecular entity or an assembly of molecules. The answer depends on how *classical* is the interaction between the two molecules. Thus, for a unitary molecular entity there is a certain degree of electronic delocalization between the acceptor atom and the hydrogen atom, while for an assembly of molecules, this interaction is mostly a Coulomb interaction.

With the concept of catastrophe theory, we can establish a working definition of a hydrogen bond as follows: "*there is a hydrogen bond when a protonated disynaptic valence basin $V(A,H)$, has a boundary with at least another valence basin, namely, $V(B)$, which does not participate to the same atomic valence shell*" [10]. Thus, in order to quantify this idea, it is defined the *core-valence bifurcation index* ν (CV index),

$$\nu(AHB) \doteq \eta(C(A), V(A,H)) - \eta(V(A,H), V(B)), \tag{2.30}$$

where $\eta(C(A), V(A,H))$ is the value of ELF at which the core basin of the donor atom A and the valence basin $V(A,H)$ bifurcate, while $\eta(V(A,H), V(B))$ is the same quantity for the basins $V(A,H)$ and $V(B)$. Then, having in mind the link between the value of the ELF in a bifurcation point and electronic delocalization between basins, one can see that $\nu(AHB)$ is a positive quantity if electrons populating the disynaptic basin $V(A,H)$ fluctuate more with the atomic core $C(A)$ than with the valence of the acceptor atom $V(B)$. In such a case the interaction in question is purely classical. On the other hand, if the electrons populating $V(A,H)$ fluctuate more with the valence $V(B)$, the interaction is a covalent one and $\nu(AHB)$ is negative.

Also, there is an empirical inverse relationship between the value of $\nu(AHB)$ and the energy of the hydrogen bond. Table 2.1 shows the values of $\nu(AHB)$ for hydrogen fluoride-nitrogen and hydrogen fluoride-ammonia dimers.

Dimer	$\eta(C(F), V(FH))$	$\eta\,(V(FH), V(N))$	$\nu\,(FHN)$
$FH--N_2$	0.149	0.047	0.102
$FH--NH_3$	0.145	0.226	-0.081

Table 2.1: Core-valence bifurcation index [10].

Also, formation energy of the $FH--N_2$ and the $FH--NH_3$ dimers are $8.6kJ/mol$ and $54.8kJ/mol$, respectively, which is consistent with the nature of the hydrogen bond in both cases: for $FH--N_2$ the hydrogen bond is purely a Coulombic interaction, while for $FH--NH_3$ the hydrogen bond corresponds to a covalent interaction.

2.2.2 Statistical tools

Once the basins the ELF are known, it is possible to perform statistical analisys on them to quantify the average of the number of electrons and how delocalized are electrons between two or more basins. The average of the electronic population of a basin Ω_A is the integral of the electronic density over the total volume of this basin,

$$\langle N(\Omega_A)\rangle = \int_{\Omega_A} \mathrm{d}\mathbf{r}\rho(\mathbf{r}). \tag{2.31}$$

Electronic fluctuation between two diferent basins is given by the elements of the covariance matrix, which are defined as [11]

$$\langle cov\,(\Omega_A, \Omega_B)\rangle = \langle N\,(\Omega_A)\rangle\,\langle N\,(\Omega_B)\rangle - \int_{\Omega_A,\Omega_B} \mathrm{d}\mathbf{r}_1\mathrm{d}\mathbf{r}_2\rho_2\,(\mathbf{r}_1, \mathbf{r}_2)\,. \tag{2.32}$$

The first term of (2.32) corresponds to a pure uncorrelated product between the electronic populations of both basins, while the second term is the actual pair population, for which it is necessary to know the form of the second-order RDM, and accounts for the correlations between the electrons of both basins. Thus, the more important the correlation term is (second term of (2.32)), the more negative the value of $\langle cov\,(\Omega_A, \Omega_B)\rangle$ is.

Chapter 3

Electron localization in excited molecular states

3.1 Linear response in density functional theory

In this chapter, we will develop the theory of linear response in time-dependent density functional theory. We will first present a standard perturbation-theory treatment based on the response of a many-particle state. Then, we will focus on the response of the electron density and, finally show how the exact many-body linear response function of the density can be computed from the independent-particle response function of the Kohn-Sham system. The last step yields to the Casida's equations of TD-DFT.

3.1.1 Perturbation theory

The dynamics of the ground state of a closed quantum system subjected to an external perturbation $\mathbf{F}$ is described by the time-dependent Schrödinger equation

$$\mathrm{i}\hbar\frac{\partial}{\partial t}\left|\Psi_0(t,\mathbf{F})\right\rangle = \left[\hat{H}^{(0)} + \lambda\hat{H}^{(1)}\right]\left|\Psi_0(t),\mathbf{F}\right\rangle, \tag{3.1}$$

where $|\Psi_0(t,\mathbf{F})\rangle$ corresponds to the ground state of the system, $\hat{H}^{(0)}$ is the unperturbed Hamiltonian (molecular Hamiltonian), $\hat{H}^{(1)}$ is the Hamiltonian due to the external perturbation, and λ is a perturbation parameter which varies continuously from 0 to 1. It is convenient to work in the interaction picture (IP) where the evolution of the ground state of the system is given by

$$\left|\Psi_0^I(t,\mathbf{F})\right\rangle = \mathrm{e}^{\mathrm{i}\hat{H}^{(0)}t}\left|\Psi_0(t,\mathbf{F})\right\rangle, \tag{3.2}$$

and the Schrödinger equation becomes

$$\mathrm{i}\frac{\partial}{\partial t}\left|\Psi_0^I(t,\mathbf{F})\right\rangle = \lambda\hat{H}_I^{(1)}(t)\left|\Psi_0^I(t),\mathbf{F}\right\rangle, \tag{3.3}$$

where $\hat{H}_I^{(1)}(t) = \mathrm{e}^{\mathrm{i}\hat{H}^{(0)}t}\hat{H}^{(1)}\mathrm{e}^{-\mathrm{i}\hat{H}^{(0)}t}$ is the perturbation Hamiltonian in the IP (hereafter, we take $\hbar = 1$). Moreover, knowing that

$$|\Psi_0^I(t), \mathbf{F}\rangle = \hat{U}_I(t, t_0)\,|\Psi_0^I(t_0)\rangle\,, \tag{3.4}$$

with $\hat{U}_I(t, t_0)$ the evolution operator in the IP and $|\Psi_0^I(t_0)\rangle \doteq |\Psi_0^{(0)}\rangle$ the ground state at $t = t_0$, the time-dependent equation for the ground state (3.3) becomes a dynamical equation for the evolution operator:

$$\mathrm{i}\frac{\partial}{\partial t}\hat{U}_I(t, t_0) = \lambda\hat{H}_I^{(1)}(t)\hat{U}_I(t, t_0). \tag{3.5}$$

If the perturbation remains small compared with the total energy of the system, an linear expansion of (3.5) in powers of λ is accurate enough,

$$\hat{U}_I(t, t_0) = 1 - \mathrm{i}\lambda\int_{t_0}^{t}\mathrm{d}t'\hat{H}_I^{(1)}(t') + O(\lambda^2). \tag{3.6}$$

After replacing Eq. 3.6 in Eq. 3.5 and then Eq. 3.5 in 3.4, one obtains the evolution to the ground state due to the external field $\mathbf{F}$,

$$|\Psi_0(t, \mathbf{F})\rangle = \mathrm{e}^{-\mathrm{i}H^0t}\,|\Psi_0^{(0)}\rangle - \mathrm{i}\lambda\mathrm{e}^{-\mathrm{i}H^0t}\int_{t_0}^{t}\mathrm{d}t'\mathrm{e}^{\mathrm{i}H^{(0)}t'}H^{(1)}\mathrm{e}^{-\mathrm{i}H^{(0)}t'}\,|\Psi_0^{(0)}\rangle + O(\lambda^2), \tag{3.7}$$

or more compactly

$$|\Psi_0(t, \mathbf{F})\rangle = |\Psi_0^{(0)}(t)\rangle + \lambda\,|\Psi_0^{(1)}(t, \mathbf{F})\rangle\,. \tag{3.8}$$

3.1.2 Linear response of the electron density

The coupling between electrons in a molecule, whose Hamiltonian does not have spin terms, and a classical radiation field with wave lengths much larger than the size of the molecules, is given by

$$\hat{H}^{(1)}(\mathbf{r}, t) = -\frac{\mathrm{e}}{m_\mathrm{e}c}\sum_{\mathrm{i}}\hat{\mathbf{p}}_i\cdot\hat{\mathbf{A}}(\mathbf{r}, t), \tag{3.9}$$

that is, it is the electric dipole momenta of the electrons $\hat{\mathbf{p}}_\mathrm{i}$ is the observable that couples with the external vector potential $\mathbf{A}(\mathbf{r}, t)$ of the radiation. Equation (3.9) can also be written in the style of DFT, i.e., in terms of the electron density and a perturbing potential $v^{(1)}$:

$$\hat{H}^{(1)}(t) = \mathbf{tr}\left[v^{(1)}\hat{\rho}\right] = \int\mathrm{d}\mathbf{r}'v^{(1)}(\mathbf{r}', t)\hat{\rho}(\mathbf{r}'). \tag{3.10}$$

The correction to the electron density $\rho(\mathbf{r})$ is just expectation value of the density operator,

$$\rho(\mathbf{r}, t) = \langle\Psi_0(t, v^{(1)})|\,\hat{\rho}(\mathbf{r})\,|\Psi_0(t, v^{(1)})\rangle\,, \tag{3.11}$$

where $|\Psi_0(t, v^{(1)})\rangle$ is the linear perturbed state (Eq. (3.7)),

$$\langle\Psi_0(t, v^{(1)})|\,\hat{\rho}(\mathbf{r})\,|\Psi_0(t, v^{(1)})\rangle = \left[\langle\Psi_0^{(0)}(t)| + \lambda\,\langle\Psi_0^{(1)}(t, v^{(1)})|\right]\hat{\rho}(\mathbf{r})\left[|\Psi_0^{(0)}(t)\rangle + \lambda\,|\Psi_0^{(1)}(t, v^{(1)})\rangle\right]. \tag{3.12}$$

After some algebra, a link between the linear evolution of the electron density and the ground many-particle state is found [45]

$$\langle\hat{\rho}(\mathbf{r})\rangle_{|\Psi_0(t,v^{(1)})\rangle} = \langle\Psi_0^{(0)}|\,\hat{\rho}_I(\mathbf{r},t)\,|\Psi_0^{(0)}\rangle - \mathrm{i}\lambda\int_{t_0}^{t}\mathrm{d}\mathbf{r}'\,\langle\Psi_0^{(0)}|\,[\hat{\rho}_I(\mathbf{r},t),\hat{H}_I^{(1)}(t')]\,|\Psi_0^{(0)}\rangle\,, \tag{3.13}$$

where $\hat{\rho}_I(\mathbf{r},t)$ is the electronic density operator in the IP. Replacing (3.10) in the commutator and taking the limits $t_0\to-\infty$ and t to ∞, one gets

$$\langle\hat{\rho}(\mathbf{r})\rangle_{|\Psi_0(t,v^{(1)})\rangle} = \langle\Psi_0^{(0)}|\,\hat{\rho}_I(\mathbf{r},t)\,|\Psi_0^{(0)}\rangle - \mathrm{i}\lambda\int_{-\infty}^{\infty}\mathrm{d}t'\mathrm{d}\mathbf{r}'\Theta(t-t')\,\langle\Psi_0^{(0)}|\,[\hat{\rho}_I(\mathbf{r},t),\hat{\rho}_I(\mathbf{r}',t')]\,|\Psi_0^{(0)}\rangle\,v^{(1)}(\mathbf{r}',t'). \tag{3.14}$$

where the step function assures time ordering (causality). From Eq. (3.14) we can define the linear response function $\chi_{\hat{\rho}\hat{\rho}}(\mathbf{r},t,\mathbf{r}',t')$ as [43]-[45]

$$\chi_{\hat{\rho}\hat{\rho}}(\mathbf{r},t,\mathbf{r}',t') = -\mathrm{i}\Theta(t-t')\,\langle\Psi_0^{(0)}|\,[\hat{\rho}_I(\mathbf{r},t),\hat{\rho}_I(\mathbf{r}',t')]\,|\Psi_0^{(0)}\rangle\,, \tag{3.15}$$

which accounts for the response of the electronic density of the unperturbed system due to the perturbing potential $v^{(1)}(\mathbf{r},t)$. The evolution of the electron density in terms of $\chi_{\hat{\rho}\hat{\rho}}$ is then given by

$$\langle\hat{\rho}(\mathbf{r})\rangle_{|\Psi_0(t,v^{(1)})\rangle} = \langle\Psi_0^{(0)}|\,\hat{\rho}_I(\mathbf{r},t)\,|\Psi_0^{(0)}\rangle + \lambda\int_{-\infty}^{\infty}\mathrm{d}t'\int\mathrm{d}\mathbf{r}'\chi_{\hat{\rho}\hat{\rho}}(\mathbf{r},t,\mathbf{r}',t')v^{(1)}(\mathbf{r}',t'). \tag{3.16}$$

Equation (3.15) is a formal definition of the linear response function, but it is not the most convenient to compute it. A more practical representation is achieved by *i*) expanding the commutator between the two densities, *ii*) applying the resolution of the identity (using energy eigenstates), *iii*) using the complex representation of the step function and *iv*) performing a pair of Fourier transformations in order to map the response to the frequency domain. After this procedure, one obtains the Lehmann representation (energy representation) of the linear response function [43],

$$\chi_{\hat{\rho}\hat{\rho}}(\mathbf{r},\mathbf{r}',\omega) = \sum_{n\neq0}^{\infty}\frac{\langle\Psi_0^{(0)}|\,\hat{\rho}(\mathbf{r})\,|\Psi_n^{(0)}\rangle\,\langle\Psi_n^{(0)}|\,\hat{\rho}(\mathbf{r}')\,|\Psi_0^{(0)}\rangle}{\omega-(E_n^{(0)}-E_0^{(0)})+\mathrm{i}\eta} - \sum_{n\neq0}^{\infty}\frac{\langle\Psi_0^{(0)}|\,\hat{\rho}(\mathbf{r}')\,|\Psi_n^{(0)}\rangle\,\langle\Psi_n^{(0)}|\,\hat{\rho}(\mathbf{r})\,|\Psi_0^{(0)}\rangle}{\omega+(E_n^{(0)}-E_0^{(0)})+\mathrm{i}\eta}. \tag{3.17}$$

The advantage of the frequency representation of $\chi_{\hat{\rho}\hat{\rho}}$ is that it is possible to extract the excitation energies of a many-particle system from the poles of $\chi_{\hat{\rho}\hat{\rho}}$. The first term in $\chi_{\hat{\rho}\hat{\rho}}$ is associated purely with the absorption of radiation and the second term associated purely with the emission. Unfortunately, determining the exact many-particle states $|\Psi_n^{(0)}\rangle$ and the exact excitation energies $\Omega_n \doteq E_n^{(0)}-E_0^{(0)}$ in realistic systems such as molecules is beyond any possibility except for very small systems. Therefore, we shall consider a different approach that allow us to determine these quantities indirectly using time dependent DFT (TD-DFT).

3.1.3 Linear response of the Kohn-Sham system

For a many-particle system it is imperative to count on approximations, like perturbation theory, that allows to access to observables of interest. In our case, the electronic density

plays a key role. In DFT the N-interactig fermionic problem is transform into an auxiliar mean-field system whose electronic density is exactly the same than the one of the real system. This auxiliar system is called the **Kohn-Sham** (KS) system [28]. Hence, instead of obtaining the first order correction to the electronic density from the interacting (real) system (Eq. (3.15)), we can write the linear change of the density as

$$\rho^{(1)}(\mathbf{r},t) = \int_{-\infty}^{\infty} \mathrm{d}t' \int \mathrm{d}\mathbf{r}' \chi_{KS}(\mathbf{r},t,\mathbf{r}',t') v_{KS}^{(1)}(\mathbf{r}',t'), \tag{3.18}$$

where χ_{KS} corresponds to the linear response function of the Kohn-Sham system and $v_{KS}^{(1)}$ is the first order correction to the mean-field potential v_{KS}, which is given by

$$v_{KS}(\mathbf{r},t) = v(\mathbf{r},t) + \int \mathrm{d}\mathbf{r}' \frac{\rho(\mathbf{r}',t)}{|\mathbf{r}-\mathbf{r}'|} + v_{xc}(\mathbf{r},t). \tag{3.19}$$

Note that the mean-field potential has a classical part, which corresponds to the external potential $v(\mathbf{r},t)$ plus the average of the electronic Coulomb repulsion (second term), and a potential that accounts for the non-classical effects, called the *exchange-correlation* potential (third term). The first term is decomposed according to $v(\mathbf{r},t) = v_0(\mathbf{r},t) + \Theta(t-t')v^{(1)}(\mathbf{r},t)$, where v_0 is the external potential due to the nuclei of the molecule and $v^{(1)}$ is the potential due to the classical radiation field. Then, an analogous equation to (3.19) holds for $v_{KS}^{(1)}$

$$v_{KS}^{(1)}(\mathbf{r},t) = v^{(1)}(\mathbf{r},t) + \int \mathrm{d}\mathbf{r}' \frac{\rho^{(1)}(\mathbf{r}',t)}{|\mathbf{r}-\mathbf{r}'|} + v_{xc}^{(1)}(\mathbf{r},t). \tag{3.20}$$

Now, from the Runge-Gross theorems, it is known that all molecular properties are functionals of the time-dependent electronic density. We know then that the exchange-correlation potential is a functional of the electronic density and hence, we can perform a functional Taylor expansion of it,

$$v_{xc}[\rho] = v_{xc}^{(0)} + \int \mathrm{d}\mathbf{r}'\mathrm{d}t' \frac{\delta v_{xc}(\mathbf{r},t)}{\delta\rho(\mathbf{r}',t')}\bigg|_{\rho^{(0)}} \rho^{(1)}(\mathbf{r}',t'), \tag{3.21}$$

where the integral in second term is nothing but $v_{xc}^{(1)}$:

$$v_{xc}^{(1)} \doteq \int \mathrm{d}\mathbf{r}'\mathrm{d}t' \frac{\delta v_{xc}(\mathbf{r},t)}{\delta\rho(\mathbf{r}',t')}\bigg|_{\rho^{(0)}} \rho^{(1)}(\mathbf{r}',t'). \tag{3.22}$$

The functional derivative in the integrand of equation (3.22) is defined as the exchange-correlation kernel [12],

$$f_{xc}(\mathbf{r},t,\mathbf{r}',t') \doteq \frac{\delta v_{xc}(\mathbf{r},t)}{\delta\rho(\mathbf{r}',t')}\bigg|_{\rho^{(0)}}; \tag{3.23}$$

which us a functional of utmost importance in TD-DFT, because it allows us to connect the auxiliar system with the real system, including information on the correlation and the exchange between electrons [12]. In particular, it is possible to find a relationship between the linear response function of the real system and its simile for the Kohn-Sham system through a Dyson-type integral equation [16]

$$\int \mathrm{d}x' \chi_{\hat{\rho}\hat{\rho}}(x,x') v^{(1)}(x') = \int \mathrm{d}x' \chi_{KS}(x,x') \left\{ v^{(1)}(x') + \int \mathrm{d}x'' \left[\frac{\delta(t'-t'')}{|\mathbf{r}'-\mathbf{r}''|} + f_{xc}(x',x'') \right] \rho^{(1)}(x'') \right\}, \tag{3.24}$$

where we have used the fact that $\rho^{(1)}$ is the same for both the real and the auxiliar system, and the notation $x \doteq (\mathbf{r}, t)$. After Fourier transformation, applying convolution theorem and reordering terms, we obtain finally the desired relationship

$$f_{xc}(\mathbf{r}, \mathbf{r}', \omega) = \chi_{KS}^{-1}(\mathbf{r}, \mathbf{r}', \omega) - \chi_{\hat{\rho}\hat{\rho}}^{-1}(\mathbf{r}, \mathbf{r}', \omega) - \frac{1}{|\mathbf{r} - \mathbf{r}'|}. \tag{3.25}$$

The major advantage in working with the Kohn-Sham system is that the linear response function χ_{KS} has a Lehmann representation in only terms of the *Kohn-Sham orbitals* $\left\{\varphi_{j\sigma}^{(0)}(\mathbf{r})\right\}$,

$$\chi_{KS}^{\sigma\sigma'}(\mathbf{r}, \mathbf{r}', \omega) = \delta_{\sigma\sigma'} \sum_{j,k} \frac{\alpha_{jk}^{\sigma}}{\omega - \omega_{jk}^{\sigma} + \mathrm{i}\eta} \varphi_{k\sigma}^{(0)*}(\mathbf{r}) \varphi_{j\sigma}^{(0)}(\mathbf{r}) \varphi_{j\sigma}^{(0)*}(\mathbf{r}') \varphi_{k\sigma}^{(0)}(\mathbf{r}'), \tag{3.26}$$

where $\alpha_{jk}^{\sigma} \doteq f_{k\sigma} - f_{j\sigma}$ are differences between occupation numbers of the spin-orbitals $\varphi_{k\sigma}$ and $\varphi_{j\sigma}$ (with $f = 1$ for an occupied orbital and $f = 0$ for empty ones), $\omega_{jk}^{\sigma} \doteq \varepsilon_{j\sigma} - \varepsilon_{k\sigma}$ are the differences of energy between respective orbitals and σ represents symbolically the spin component of the spin-orbitals ($\sigma = |+\rangle$ or $|-\rangle$).

3.1.4 Casida's equations

From now on we consider explicitly the spin-dependence in the electronic density, and we assume from the beginning that $v^{(1)} = 0$. The reason is that here we are interested in the eigenmodes and eigenfrecquencies of the system, that is, how is the response of the system to a perturbation happened in the distant past. In other words, we are interested in the density of the stationary state that the system achieves after the absorption of radiation. Hence, using (3.18), the first order correction to the density of electrons with σ spin, in the frequency domain, is [16]

$$\rho_{\sigma}^{(1)}(\mathbf{r}, \Omega) = \sum_{\sigma', \sigma''} \int \mathrm{d}\mathbf{r}' \chi_{KS}^{\sigma\sigma'}(\mathbf{r}, \mathbf{r}', \Omega) \int \mathrm{d}\mathbf{r}'' f_{Hxc}^{\sigma'\sigma''}(\mathbf{r}', \mathbf{r}'', \Omega) \rho_{\sigma''}^{(1)}(\mathbf{r}'', \Omega). \tag{3.27}$$

For simplicity we have defined f_{Hxc} as

$$f_{Hxc}(\mathbf{r}, \mathbf{r}', \Omega) \doteq f_{xc}(\mathbf{r}, \mathbf{r}', \Omega) + \frac{1}{|\mathbf{r} - \mathbf{r}'|}. \tag{3.28}$$

Multiplying (3.27) by f_{Hxc}, and using the definition of its expected value,

$$\left\langle f_{Hxc}^{\sigma\sigma'}(\mathbf{r}, \mathbf{r}', \Omega) \right\rangle_{\rho_{\sigma'}^{(1)}(\mathbf{r}', \Omega)} = \int \mathrm{d}\mathbf{r}' f_{Hxc}^{\sigma\sigma'}(\mathbf{r}, \mathbf{r}', \Omega) \rho_{\sigma'}^{(1)}(\mathbf{r}', \Omega) \tag{3.29}$$

$$\doteq g_{\sigma\sigma'}(\mathbf{r}, \Omega), \tag{3.30}$$

we obtain

$$g_{\sigma'''\sigma}(\mathbf{r}''', \Omega) = \int \mathrm{d}\mathbf{r} f_{Hxc}^{\sigma'''\sigma}(\mathbf{r}''', \mathbf{r}, \Omega) \sum_{\sigma'\sigma''} \int \mathrm{d}\mathbf{r}' \chi_{KS}^{\sigma\sigma'}(\mathbf{r}, \mathbf{r}', \Omega) g_{\sigma'\sigma''}(\mathbf{r}', \Omega). \tag{3.31}$$

Now, using (3.26) in the equation above, and defining the matrix elements $H_{jk,\sigma}$ as

$$H_{jk,\sigma}(\Omega) = \sum_{\sigma'} \langle \varphi^{(0)}_{j,\sigma}| \left\langle f^{\sigma\sigma'}_{Hxc} \right\rangle_{\rho^{(1)}_{\sigma'}} |\varphi^{(0)}_{k,\sigma}\rangle \,, \tag{3.32}$$

we obtain, after rearranging index conveniently, the following iterative equation

$$H_{jk,\sigma}(\Omega) = \sum_{\sigma'} \sum_{j',k'} \frac{\alpha^{\sigma'}_{j'k'}}{\Omega - \omega^{\sigma'}_{j'k'}} K^{k'j',\sigma'}_{jk,\sigma}(\Omega) H_{j'k',\sigma'}(\Omega) \tag{3.33}$$

where $K^{k'j',\sigma'}_{jk,\sigma}(\Omega)$ are the two-particle matrix elements of f_{Hxc}, which are given by

$$K^{k'j',\sigma'}_{jk,\sigma'}(\Omega) \doteq \langle \varphi^{(0)}_{j\sigma}, \varphi^{(0)}_{k'\sigma'}| \, f^{\sigma\sigma'}_{Hxc} \, |\varphi^{(0)}_{k\sigma}, \varphi^{(0)}_{j'\sigma'}\rangle \,. \tag{3.34}$$

Then, multiplying both sides of (3.33) by $(\Omega - \omega^{\sigma}_{jk})^{-1}$ and defining $\beta_{jk,\sigma}(\Omega)$ as

$$\beta_{jk,\sigma}(\Omega) \doteq \frac{H_{jk,\sigma}(\Omega)}{\Omega - \omega^{\sigma}_{jk}}, \tag{3.35}$$

we obtain, after rearranging terms,

$$\Omega\beta_{jk,\sigma}(\Omega) = \sum_{\sigma'} \sum_{j'k'} \left[\delta_{\sigma\sigma'}\delta_{jj'}\delta_{kk'}\omega^{\sigma'}_{j'k'} + \alpha^{\sigma'}_{j'k'} K^{k'j',\sigma'}_{jk,\sigma}(\Omega) \right] \beta_{j'k',\sigma'}(\Omega). \tag{3.36}$$

Now, as a KS orbital can be occupied (hole state) or empty (particle state), we explicitly use i for labeling occupied orbitals and a for empty ones:

$$\begin{aligned}
\Omega\beta_{ai,\sigma} &= \sum_{\sigma'} \sum_{a'i'} \left\{ \left[\delta_{\sigma\sigma'}\delta_{aa'}\delta_{ii'}\omega^{\sigma'}_{a'i'} + K^{i'a',\sigma'}_{ai,\sigma} \right] \beta_{a'i',\sigma'} - K^{a'i',\sigma'}_{ai,\sigma} \beta_{i'a',\sigma'} \right\}, \\
\Omega\beta_{ia,\sigma} &= \sum_{\sigma'} \sum_{a'i'} \left\{ \left[\delta_{\sigma\sigma'}\delta_{aa'}\delta_{ii'}\omega^{\sigma'}_{i'a'} - K^{a'i',\sigma'}_{ia,\sigma} \right] \beta_{i'a',\sigma'} + K^{i'a',\sigma'}_{ia,\sigma} \beta_{a'i',\sigma'} \right\},
\end{aligned} \tag{3.37}$$

where we use $\alpha^{ai}_{ia} = \pm 1$ to separate the sum. Note that in Eq. (3.37) only particle-hole excitation ($i \to a$) or deexcitation ($a \to i$) are present. Therefore, processes that imply double or higher excitations are not captured by linear response TD-DFT (LR-TDDFT). Finally, defining conveniently the matrices $X_{ia,\sigma}$ and $Y_{ia,\sigma}$ as

$$X_{ia,\sigma} \doteq \beta_{ai,\sigma}, \quad Y_{ia,\sigma} \doteq -\beta_{ia,\sigma}, \tag{3.38}$$

and the fourth-rank tensors $\mathbf{A}$ and $\mathbf{B}$, whose components are given by

$$A^{i'a',\sigma'}_{ia,\sigma} \doteq \delta_{ii'}\delta_{aa'}\delta_{\sigma\sigma'}\omega^{\sigma'}_{a'i'} + K^{i'a',\sigma'}_{ai,\sigma}, \tag{3.39}$$

$$B^{i'a',\sigma'}_{ia,\sigma} \doteq K^{i'a',\sigma'}_{ia,\sigma}, \tag{3.40}$$

we recast Eq. (3.37) into a general matricial form, know as the *Casida's equations* (CE) [14]-[16],

$$\begin{bmatrix} \mathbf{A} & \mathbf{B}^T \\ \mathbf{B} & \mathbf{A}^T \end{bmatrix} \begin{bmatrix} \mathbf{X} \\ \mathbf{Y} \end{bmatrix} = \Omega \begin{bmatrix} \mathbf{I} & \mathbf{0} \\ \mathbf{0} & -\mathbf{I} \end{bmatrix} \begin{bmatrix} \mathbf{X} \\ \mathbf{Y} \end{bmatrix}. \tag{3.41}$$

CE gives, in principle, the exact excitation energies for any molecular system, via the poles of the Kohn-Sham linear response function χ_{KS}, $\Omega = \omega_{jk}$, which in the self-consistent procedure converges to the poles of $\chi_{\hat{\rho}\hat{\rho}}$ of the real system, Ω_n. The only approximation involved in CE is the approximation used for the exchange-correlation potential. Note that CE only depends on the orbitals and excitation energies of the Kohn-Sham system, ω_{jk}, which are standard outputs of a ground state DFT calculation. Although CE treats explicitly only single excitations and deexcitations, higher order many-body effects are included, in an averaged way, by the exchange-correlation kernel. An important simplification of CE consists in neglecting the $\mathbf{B}$ tensor in (3.41), that is, considering excitations only. This simplification is called the *Tamm-Dancoff approximation* [13], and the empirical evidence shows that for gradient-generalized exchange-correlation functionals (GGA), it yields to better excitation energies than the full CE but it gives wrong oscillator strengths [17]. Furthermore, other properties, such as the electron density of excited states do not necessarily improve with Tamm-Dancoff approximation.

Summarizing, the first order correction to the ground state density (3.27) after excitation to the n-excited state, in the linear regime, can be written in terms of the matrix elements $X_{ia,\sigma}$ and $Y_{ia,\sigma}$ and the KS orbitals:

$$\rho_\sigma^{(1)}(\mathbf{r}, \Omega_n) = \sum_{i,a} \left[\varphi_{a,\sigma}^{(0)}(\mathbf{r}) \varphi_{i,\sigma}^{*(0)}(\mathbf{r}) X_{ia,\sigma} + \varphi_{i,\sigma}^{*(0)}(\mathbf{r}) \varphi_{a,\sigma}^{(0)}(\mathbf{r}) Y_{ia,\sigma} \right], \tag{3.42}$$

where the first term of (3.42) corresponds to single excitations and the second one to single deexcitations. Thus, the density of the n-excited state is just

$$\rho_{n,\sigma}(\mathbf{r}, \Omega) = \rho_\sigma^{(0)}(\mathbf{r}, \Omega) + \rho_{\sigma,n}^{(1)}(\mathbf{r}, \Omega), \tag{3.43}$$

where $\rho_\sigma^{(0)}(\mathbf{r}, \Omega) = \langle \Psi_0^{(0)}(\Omega) | \, \hat{\rho}_\sigma(\mathbf{r}) \, | \Psi_0^{(0)}(\Omega) \rangle$.

It should be noted that we use the term deexcitation as a synonymous of stimulated emission. Remember that we consider the molecule as a closed system; hence, spontaneous emission cannot occur.

3.2 Electronic correlation in DFT

A molecule in an excited state has often a high electronic correlation, mainly because the many-particle wave function is more delocalized than in the ground state and because the chances of an excited state to mix with another one is large. Besides, although the correlation energy contribution to the total energy of the ground state may be small, it could be equal or larger than the excitation energies. Hence, the ideal is to treat correlation energy in the ground and excited states with the same accuracy. Nevertheless, this is not often the case as correlation in an excited state is usually more difficult to capture.

Calculations of molecular excited states with TD-DFT precises the choice of a functional that approximates the *exchange-correlation energy* $E_{xc}[\rho]$, which is defined within DFT as [28]

$$E_{xc}[\rho] \doteq (T[\rho] - T_{KS}[\rho]) + (V_{\text{ee}}[\rho] - V_{KS}[\rho]), \tag{3.44}$$

where $T[\rho]$ and $V[\rho]$ are the kinetic energy functional and the interelectronic repulsion functional of the real system, and $T_{KS}[\rho]$ and $V_{KS}[\rho]$ are the same quantities for the mean-field KS system, whose expressions in terms of the KS orbitals, $\{\varphi_{\mathrm{i}}\}$, are given by

$$T_{KS}[\rho] = \sum_{i=1}^{N} \langle \varphi_i | \left(-\frac{1}{2}\nabla_i^2 \right) | \varphi_i \rangle \,, \tag{3.45}$$

$$V_{KS}[\rho] = V_{class} = \int \mathrm{d}\mathbf{r}' \frac{\rho(\mathbf{r}')}{|\mathbf{r} - \mathbf{r}'|}. \tag{3.46}$$

"Standard" functional in DFT, such as those based on the *generalized gradient approximation* (GGA) [30] do not describe the correct long-range behavior of the exchange potential $(1/r)$. Rather, they predict an exponential decay, which results in KS orbitals too high in energy and KS excitation energies to far from the actual excitation energies [16]. Thus, in the treatment of excitations with TD-DFT, functionals with the correct long-range behavior are necessary. In this work, we use a *long-range hybrid functional*.

In the rest of this section we first briefly review the two kinds of electronic correlation that one finds in molecular systems, namely, static and dynamical correlation. Then, with the purpose to perform analysis of electronic localization, based on ELF, in excited states, we will define the quantities that will allow us to reconstruct the second-order RDM in interacting systems.

3.2.1 Static vs dynamical correlation

Although we will use DFT all along this work, it is convenient to discuss correlation energy within the framework of wave function-based methods. In a wave function method, the correlation energy is defined as the missing part in the mean-field approximation of HF [29]-[33],

$$E_c = E_{exact} - E_{HF}. \tag{3.47}$$

Note that when a wave function method is used, the exchange energy is not included as a correlation energy. The exchange correlation between electrons of the same spin appears naturally in HF as a direct consequence of the Pauli exclusion principle. In mono-determinantal approximations, such as HF, a electron sees other electrons as a mean field produced by them. But, classically speaking, electrons move such that they instantaneously avoid locations taken by other electrons. The piece of correlation energy that HF fails to capture due to this instantaneous dynamics of electrons is called *dynamical correlation energy* [29]. The effect of dynamical correlation energy is decreasing the energy below the HF limit. Dynamical correlation can be included starting from the HF approximation by adding more Slater determinants to the trial wave function. These additional determinants are constructed from the single determinant of the HF ground state $|\Psi_0\rangle$ by creating new determinants that are excitations from occupied, $\{|\psi_{i,\sigma}\rangle\}$, to unoccupied spin orbitals $\{|\psi_{a,\sigma}\rangle\}$. These extra determinants, which can correspond to single, double or multiple excitations, can be used along

with $|\Psi_0\rangle$, to build a more accurate wave function for the ground state of the many-particle system, that is to say,

$$|\Psi\rangle = c_0 |\Psi_0\rangle + \sum_{i,a} c_i^a |\Psi_i^a\rangle + \left(\frac{1}{2!}\right)^2 \sum_{i,a} \sum_{j,b} c_{ij}^{ab} |\Psi_{ij}^{ab}\rangle + ... \tag{3.48}$$

The above expression is the well-known CI (configuration interaction) expansion [29].

Sometimes the HF ground state may not be a good mean field reference to construct a CI wave function. That is the case, for instance, when the ground state is degenerate or pseudo-degenerate (molecules with transition metal with partially filled d states). The piece of correlation energy that HF fails to capture in this case is called *static correlation energy.*

In density functional theory, particulary, in the KS system, the electron density is given by

$$\rho(\mathbf{r}) = \sum_{i=1}^{N} |\varphi_i(\mathbf{r})|^2, \tag{3.49}$$

where $\{\varphi_i(\mathbf{r})\}$ is a basis of KS orbitals, which are solutions of the KS equations:

$$\left[-\frac{1}{2}\nabla_{\mathbf{r}}^2 + v_{KS}(\mathbf{r})\right] \varphi_i(\mathbf{r}) = \varepsilon_i \varphi_i(\mathbf{r}). \tag{3.50}$$

Here, $v_{KS}(\mathbf{r})$ is the ground state (time-independent) KS potential, which is directly related to the exchange-correlation potential $v_{xc}(\mathbf{r})$ (Eq. (3.19)). Thus, the exchange-correlation effects are include in the electron density through $v_{xc}(\mathbf{r})$, which is related with E_{xc} by

$$v_{xc}[\rho] = \frac{\delta E_{xc}[\rho]}{\delta \rho}. \tag{3.51}$$

Moreover, the KS system is also a single Slater determinant of KS orbitals. Therefore, except in the case that one knows the exact exchange-correlation functional, static correlation is very difficult of including or tuning the amount of it present in each approximate exchange-correlation functional.

In the time dependent counterpart (TD-DFT), exchange and correlation effects between particles and holes are encoded in exchange-correlation kernel, f_{xc}, which is the second functional derivative of the exchange-correlation energy with respect to the density

$$f_{xc}(\mathbf{r}, t, \mathbf{r}', t') = \frac{\delta}{\delta \rho(\mathbf{r}', t')} \frac{\delta E_{xc}[\rho]}{\delta \rho(\mathbf{r}, t)}\bigg|_{\rho^{(0)}}. \tag{3.52}$$

Note that in the CE exchange and correlation are included through f_{xc} in the eigenvectors $X_{ia,\sigma}$ and $Y_{ia,\sigma}$. Therefore, from (3.42) one concludes that in TD-DFT the first order correction of the electronic density is given by a correlated (CI-like) expansion of the KS orbitals.

Given the mono-determinantal nature of DFT and HF, there is a similarity between the TD-DFT equations (CE) and those of the time-dependent Hartree-Fock (TD-HF) method. This similarity is easy to see in the cases of hybrid exchange-correlation functionals, which

include a fraction HF exchange. For example, if one considers an exchange-correlation functional composed purely by Hartree exchange, that is, taking $v_{xc} = v_x^{HF}$, one recovers the equations of TD-HF [13]. In other words, starting from the time-dependent Schrödinger equation for a Slater determinant,

$$\mathrm{i}\frac{\partial}{\partial t}\left|\psi_i(\mathbf{r},t)\right\rangle = \left[-\frac{1}{2}\nabla^2 + v(\mathbf{r},t)\right]\left|\psi_i(\mathbf{r},t)\right\rangle + \sum_{j=1}^{N}\left[\hat{V}_j(\mathbf{r}') - \hat{K}_j(\mathbf{r}')\right]\left|\psi_i(\mathbf{r},t)\right\rangle, \tag{3.53}$$

where $\hat{V}_j$ and $\hat{K}_j$ are the coulomb and exchange operators, respectively, which are defined through the action on a spin-orbital $|\psi_i(\mathbf{r},t)\rangle$ as

$$\hat{V}_j(\mathbf{r}')\left|\psi_i(\mathbf{r},t)\right\rangle = \left\langle\psi_j(\mathbf{r}',t)\right| \frac{1}{|\mathbf{r}-\mathbf{r}'|}\left|\psi_j(\mathbf{r}',t)\right\rangle\left|\psi_i(\mathbf{r},t)\right\rangle, \tag{3.54}$$

$$\hat{K}_j(\mathbf{r}')\left|\psi_i(\mathbf{r},t)\right\rangle = \left\langle\psi_j(\mathbf{r}',t)\right| \frac{1}{|\mathbf{r}-\mathbf{r}'|}\left|\psi_i(\mathbf{r}',t)\right\rangle\left|\psi_j(\mathbf{r},t)\right\rangle, \tag{3.55}$$

it is possible to obtain a matrix equation with the same form of the CE, the only difference being that in TD-HF there is not exchange-correlation kernel but a purely non-local mean-field potential. Also, if one applies the Tamm-Dancoff approximation to the TD-HF equations, one recovers the simplest wave function method for the calculation of excitation energies in molecules: *configuration interaction singles* (CIS) [35]. CIS method outputs excitation energies after diagonalizing the molecular Hamiltonian written in a basis of all Slater determinants that are a single excitation of the HF determinant; that is, the CI expansion (3.48) truncated in the first summation.

Summarizing, TD-DFT with approximate functionals include dynamical correlation and they could fail to include static correlation, although empirical results show that TD-DFT with hybrid-long-range corrected functional qualitatively describe conical intersections between the ground and first excited state [14].

3.3 ELF and natural orbitals

In mean-field systems, like HF or KS systems, the first-order RDM is diagonalized by the canonical spin-orbitals or by the KS orbitals, respectively,

$$\hat{\gamma}_1 = \sum_i n_i \left|\psi_i\right\rangle\left\langle\psi_i\right|, \tag{3.56}$$

where n_i are the occupation numbers. However, in real (interacting) fermion systems, where its N-particle state is not described by a slater determinant, $\hat{\gamma}_1$ is not diagonalizable by these sets of orbitals, so that

$$\hat{\gamma}_1 = \sum_{i,j} n_{ij} \left|\psi_i\right\rangle\left\langle\psi_j\right|. \tag{3.57}$$

Fortunately, one can always perform a unitary transformation from the set of mean-field states $\{|\psi_i\rangle\}$ to another set $\{|\eta_i\rangle\}$, which allows us to diagonalize $\hat{\gamma}_1$ in interacting (and correlated) systems, i.e.,

$$\hat{\gamma}_1 = \sum_i \lambda_i \left|\eta_i\right\rangle\left\langle\eta_i\right|. \tag{3.58}$$

This basis corresponds to the *natural orbital* basis set, and form an eigenbasis for $\hat{\gamma}_1$ in correlated systems [29]-[32]. Note that both (3.56) and (3.58) have the same form. However, they differs in the occupation numbers. In the noninteracting case, the occupation numbers takes the value 1 for occupied orbitals, and 0 for virtual ones, and hence, $\hat{\gamma}_1$ is idempotent (so the sum in (3.56) goes up to N). On the other hand, occupation numbers λ_i of the interacting systems are fractional numbers between 0 and 1, so that $\hat{\gamma}_1$ is not idempotent. Then, we will use natural orbitals to approximate the second-order RDM.

The importance of knowing an approximate form of the second-order RMD in correlated systems as molecular excited states is twofold. First, the delocalization field of the ELF ($D(\mathbf{r})$) comes from the spherical average of the conditional pair probability $P(\mathbf{r}_2|\mathbf{r}_1)$ which is directly related to ρ_2. Second, in order to perform ELF analysis in excited states, we require the explicit form of both first and second-order RDMs. Thus, electronic population over a certain basin $\langle N(\Omega)\rangle$ is calculated through the integration of the electronic density, whose first-order correction is given by (3.42), while the covariances between basins are calculated using both, the electronic density, and ρ_2. However, due to the dynamical correlation of excited states, there is no exact analytical decomposition of $\hat{\gamma}_2$ in terms of $\hat{\gamma}_1$, unlike HF systems.

A general approximate form of a second-order RDM in terms of the first order RDM, can be written as [5]

$$\rho_{2\sigma}(\mathbf{r}_1,\mathbf{r}_2) = \rho_\sigma(\mathbf{r}_1)\rho_\sigma(\mathbf{r}_2) - |\rho_{1\sigma}(\mathbf{r}_1,\mathbf{r}_2)|^2 + \xi_{2\sigma}(\mathbf{r}_1,\mathbf{r}_2), \tag{3.59}$$

where $\xi_{2\sigma}(\mathbf{r}_1,\mathbf{r}_2)$ is the correlation correction. Then, there are several reconstructions of $\hat{\gamma}_2$ with different degrees of complexity. The simpler one, is the HF reconstruction in which one assumes $\xi_{2\sigma}(\mathbf{r}_1,\mathbf{r}_2) = 0$, obtaining thus a HF-like decomposition of $\rho_{2\sigma}(\mathbf{r}_1,\mathbf{r}_2)$, in terms of natural orbitals (instead of HF spin-orbitals or KS orbitals):

$$\rho_{2\sigma}(\mathbf{r}_1,\mathbf{r}_2) = \sum_{i,j}\lambda_i\lambda_j\left[\eta^*_{i\sigma}(\mathbf{r}_1)\eta^*_{j\sigma}(\mathbf{r}_2)\eta_{i\sigma}(\mathbf{r}_1)\eta_{j\sigma}(\mathbf{r}_2) - \eta^*_{i\sigma}(\mathbf{r}_1)\eta^*_{j\sigma}(\mathbf{r}_2)\eta_{j\sigma}(\mathbf{r}_1)\eta_{i\sigma}(\mathbf{r}_2)\right]. \tag{3.60}$$

This approximation for the second-order RDM fulfills the Pauli principle [28],

$$\rho_{2\sigma}(\mathbf{r}_1;\mathbf{r}_1) = 0, \tag{3.61}$$

and the electron-electron cusp condition [34]

$$\nabla_{\mathbf{r}_2}\rho_{2\sigma}(\mathbf{r}_1;\mathbf{r}_2)|_{\mathbf{r}_1=\mathbf{r}_2} = 0. \tag{3.62}$$

It is worth mentioning that is desirable that an approximation for second-order RDM fulfills these two conditions, because they contain the basic rules of the dynamics of electron of the same spin.

In the following, we show with some detail, the deduction of the delocalization field $D_\sigma(\mathbf{r})$ for molecular excited states, i.e., using the HF-like reconstruction for $\rho_{2\sigma}$ and expressing this in terms of natural orbitals. The associated conditional pair probability for (3.59) is given by

$$P(\mathbf{r}_2,\sigma|\mathbf{r}_1,\sigma) = \rho_\sigma(\mathbf{r}_2) + 2\rho_{x\sigma}(\mathbf{r}_1,\mathbf{r}_2), \tag{3.63}$$

where $\rho_{x\sigma}$ is the exchange density defined in Eq. (2.17).

The short range (small $|\mathbf{r}_1 - \mathbf{r}_2|$) part of $P(\mathbf{r}_2, \sigma|\mathbf{r}_1, \sigma)$ has most of the information on the Pauli repulsion between electrons. This short-range information can be exctracted by performing a Taylor expansion and, assuming that there is an electron located in a reference point $\mathbf{r} = \mathbf{r}_1$ and taking the limit where the second electron is close to the first one to a distance $s = |\mathbf{r}_2 - \mathbf{r}_1| \to 0$. Thus, considering the expansion of the electron density, up to a linear term in $\mathbf{s}$,

$$\begin{aligned}\rho_\sigma(\mathbf{r}+\mathbf{s}) &= \rho_\sigma(\mathbf{r}) + \mathbf{s}\cdot\nabla_\mathbf{s}\rho_\sigma(\mathbf{r}+\mathbf{s})\Big|_{\mathbf{s}=0} + O(\mathbf{s}^2), \\ &= \mathrm{e}^{\mathbf{s}\cdot\nabla_\mathbf{s}}\rho_\sigma(\mathbf{r}+\mathbf{s})\Big|_{\mathbf{s}=0}, \end{aligned} \tag{3.64}$$

and taking the spherical average

$$\langle\rho_\sigma(\mathbf{r}+\mathbf{s})\rangle = \left\langle \mathrm{e}^{\mathbf{s}\cdot\nabla_\mathbf{s}}\right\rangle \rho_\sigma(\mathbf{r}+\mathbf{s})\Big|_{\mathbf{s}=0}, \tag{3.65}$$

we obtain

$$\langle\rho_\sigma(\mathbf{r}+\mathbf{s})\rangle = \rho_\sigma(\mathbf{r}) + \frac{s^2}{3!}\nabla^2_\mathbf{s}\rho_\sigma(\mathbf{r}+\mathbf{s})\Big|_{\mathbf{s}=0}. \tag{3.66}$$

The spherical average entails an integration over a solid angle $\mathrm{d}\Omega = sin\theta\mathrm{d}\theta\mathrm{d}\phi$ for a fixed interelectronic distance s, i.e.,

$$\left\langle \mathrm{e}^{\mathbf{s}\cdot\nabla_\mathbf{s}}\right\rangle = \frac{1}{4\pi}\int \mathrm{e}^{\mathbf{s}\cdot\nabla_\mathbf{s}} sin\theta\mathrm{d}\theta\mathrm{d}\phi, \tag{3.67}$$

$$= \frac{sinh(\|\mathbf{s}\|\|\nabla_\mathbf{s}\|)}{\|\mathbf{s}\|\|\nabla_\mathbf{s}\|}, \tag{3.68}$$

where we also have used the expansion of the hyperbolic sine,

$$sinh(x) = \sum_{n=0}^{\infty}\frac{x^{2n+1}}{(2n+1)!}. \tag{3.69}$$

In the same form, it is possible to show that the spherical average of the exchange density is:

$$\begin{aligned}\langle\rho_{x\sigma}(\mathbf{r},\mathbf{r}+\mathbf{s})\rangle &= \left[1 + \frac{s^2\nabla^2_\mathbf{s}}{3!} + O(s^4)\right]\rho_{x\sigma}(\mathbf{r},\mathbf{r}+\mathbf{s})\Big|_{\mathbf{s}=0}, \\ &= -\frac{1}{2}\rho_\sigma(\mathbf{r}) + \frac{s^2}{3!}\nabla^2_\mathbf{s}\rho_{x\sigma}(\mathbf{r},\mathbf{r}+\mathbf{s})\Big|_{\mathbf{s}=0} + O(s^4), \end{aligned} \tag{3.70}$$

where we have used the fact that $\rho_{x\sigma}(\mathbf{r},\mathbf{r}) = -\frac{1}{2}\rho_\sigma(\mathbf{r})$. Hence, the spherical average of conditional pair probability is written as

$$\langle P(\mathbf{r}+\mathbf{s},\sigma|\mathbf{r},\sigma)\rangle = \frac{s^2}{3!}\nabla^2_\mathbf{s}\left[\rho_\sigma(\mathbf{r}+\mathbf{s}) + 2\rho_{x\sigma}(\mathbf{r},\mathbf{r}+\mathbf{s})\right]\Big|_{\mathbf{s}=0} + O(s^4). \tag{3.71}$$

Now, in order to compute the Laplacians, we express $\rho_{1\sigma}$ in terms of natural orbitals,

$$\rho_{1\sigma}(\mathbf{r}_1,\mathbf{r}_2)=\sum_i \lambda_i \eta_{i\sigma}(\mathbf{r}_1)\eta^*_{i\sigma}(\mathbf{r}_2). \tag{3.72}$$

Assuming real orbitals, we obtain for the Laplacian of the electron density:

$$\nabla^2_{\mathbf{s}}\rho_\sigma(\mathbf{r}+\mathbf{s})=2\sum_i \lambda_i|\nabla_{\mathbf{s}}\eta_{i\sigma}(\mathbf{r}+\mathbf{s})|^2+2\sum_i \lambda_i\eta_{i\sigma}(\mathbf{r}+\mathbf{s})\nabla^2_{\mathbf{s}}\eta_{i\sigma}(\mathbf{r}+\mathbf{s}). \tag{3.73}$$

On the other hand, the Laplacian of the exchange density, results

$$\nabla^2_{\mathbf{s}}\rho_{x\sigma}(\mathbf{r},\mathbf{r}+\mathbf{s})=-\frac{1}{\rho_\sigma(\mathbf{r})}\left[\rho_{1\sigma}(\mathbf{r},\mathbf{r}+\mathbf{s})\nabla^2_{\mathbf{s}}\rho_{1\sigma}(\mathbf{r},\mathbf{r}+\mathbf{s})+\nabla_{\mathbf{s}}\rho_{1\sigma}(\mathbf{r},\mathbf{r}+\mathbf{s})\cdot\nabla_{\mathbf{s}}\rho_{1\sigma}(\mathbf{r},\mathbf{r}+\mathbf{s})\right]. \tag{3.74}$$

Summing (3.73) and (3.74), taking the limit $\mathbf{s}=0$ ($\mathbf{r}_1=\mathbf{r}_2$), and returning to the original variables $\mathbf{r}_1$ and $\mathbf{r}_2$,

$$\begin{aligned}\langle P(\mathbf{r}+\mathbf{s},\sigma|\mathbf{r},\sigma)\rangle &= \frac{s^2}{3}\left[\sum_i \lambda_i|\nabla_{\mathbf{s}}\eta_{i\sigma}(\mathbf{r}+\mathbf{s})|^2-\frac{|\nabla_{\mathbf{s}}\rho_{1\sigma}(\mathbf{r},\mathbf{r}+\mathbf{s})|^2}{\rho_\sigma(\mathbf{r})}\right]\Bigg|_{\mathbf{s}=0},\\ &= \frac{s^2}{3}\left[\sum_i \lambda_i|\nabla_{\mathbf{r}_2}\eta_{i\sigma}(\mathbf{r}_2)|^2-\frac{|\nabla_{\mathbf{r}_2}\rho_{1\sigma}(\mathbf{r}_2,\mathbf{r}_2)|^2}{\rho_\sigma(\mathbf{r}_2)}\right].\end{aligned} \tag{3.75}$$

Finally, renaming $\mathbf{r}_2$ simply by $\mathbf{r}$, we obtain for the spherical average of the conditional pair probability,

$$\langle P(\mathbf{r},\sigma|\mathbf{r}_1,\sigma)\rangle=\frac{s^2}{3}\left[\sum_i \lambda_i|\nabla_{\mathbf{r}}\eta_{i\sigma}(\mathbf{r})|^2-\frac{|\nabla_{\mathbf{r}}\rho_\sigma(\mathbf{r})|^2}{\rho_\sigma(\mathbf{r})}\right]=\frac{s^2}{3}D^{HF}_\sigma(\mathbf{r}), \tag{3.76}$$

where, in the bosonic term (the second one), we have used the fact that $\rho_{1\sigma}(\mathbf{r},\mathbf{r})=\rho_\sigma(\mathbf{r})$. The principal difference between the delocalization field of a HF system (Eq. (2.21)) and its correlated reconstruction written in terms of natural orbitals, is that the sum in the kinetic electronic density goes, in principle, up to infinity, while in HF goes up to $N/2$.

Here, we have introduced the electronic correlation through natural orbitals and its fractional occupation numbers λ_i. However, there are other approaches more sophisticated than the HF-like reconstruction of ρ_2, in which the correlation correction $\xi_{2\sigma}$ is different from zero. Buijse and Baerends showed that a good choice for $\xi_{2\sigma}$ (BB correlation correction term) is given by [5]

$$\xi_{2\sigma}(\mathbf{r}_1,\mathbf{r}_2)=\sum_{i,j}\left(\lambda_i\lambda_j-\sqrt{\lambda_i\lambda_j}\right)\eta^*_{i\sigma}(\mathbf{r}_1)\eta^*_{j\sigma}(\mathbf{r}_2)\eta_{j\sigma}(\mathbf{r}_1)\eta_{i\sigma}(\mathbf{r}_2), \tag{3.77}$$

where the difference $\lambda_i\lambda_j-\sqrt{\lambda_i\lambda_j}$ is a measure of dynamic correlations. Note that for HF or KS systems, due to $\lambda_i=0$ for occupied orbitals, $\lambda_i\lambda_j=\sqrt{\lambda_i\lambda_j}$, and hence $\xi_{2\sigma}=0$. In general, we can use an arbitrary function of the occupation numbers that fulfills the condition $f(\lambda_i\lambda_j)=\lambda_i\lambda_j$, for $\lambda_i=\lambda_j=1$. In such a case, the conditional pair probability is given by

$$P(\mathbf{r}_2,\sigma|\mathbf{r}_1,\sigma)=\rho_\sigma(\mathbf{r}_2)-\frac{|\rho_{1\sigma}(\mathbf{r}_1,\mathbf{r}_2)|^2}{\rho_\sigma(\mathbf{r}_1)}+\sum_{i,j}\frac{(\lambda_i\lambda_j-f(\lambda_i,\lambda_j))}{\rho_\sigma(\mathbf{r}_1)}\eta^*_{i\sigma}(\mathbf{r}_1)\eta^*_{j\sigma}(\mathbf{r}_2)\eta_{j\sigma}(\mathbf{r}_1)\eta_{i\sigma}(\mathbf{r}_2). \tag{3.78}$$

Now, we calculate the spherical average of (3.78). Defining

$$\xi'_{2\sigma}(\mathbf{r}_1,\mathbf{r}_2) \doteq \frac{\xi_{2\sigma}(\mathbf{r}_1,\mathbf{r}_2)}{\rho_\sigma(\mathbf{r}_1)}, \tag{3.79}$$

and proceeding in the same way, i.e., changing $\mathbf{r}_1$ and $\mathbf{r}_2$ by $\mathbf{r}$ and $\mathbf{s}$, we obtain for the spherical average of $\xi'_{2\sigma}$,

$$\begin{aligned}\langle \xi'_{2\sigma}(\mathbf{r},\mathbf{r}+\mathbf{s})\rangle &= \xi'_{2\sigma}(\mathbf{r},\mathbf{r}) + \frac{s^2}{3!}\nabla^2_{\mathbf{s}}\xi'_{2\sigma}(\mathbf{r},\mathbf{r}+\mathbf{s})\Big|_{\mathbf{s}=0} + O(s^4) \\ &= \frac{\sum_{i,j}\left(\lambda_i\lambda_j - f(\lambda_i,\lambda_j)\right)|\eta_{i\sigma}(\mathbf{r})|^2|\eta_{j\sigma}(\mathbf{r})|^2}{\sum_k \lambda_k|\eta_{k\sigma}(\mathbf{r})|^2} \\ + \frac{s^2}{3!}&\frac{\sum_{i,j}\left(\lambda_i\lambda_j - f(\lambda_i,\lambda_j)\right)\eta^*_{i\sigma}(\mathbf{r})\eta_{j\sigma}(\mathbf{r})\left[2\nabla_{\mathbf{s}}\eta_{i\sigma}\cdot\nabla_{\mathbf{s}}\eta^*_{j\sigma} + \eta_{i\sigma}\nabla^2_{\mathbf{s}}\eta^*_{j\sigma} + \eta^*_{j\sigma}\nabla^2_{\mathbf{s}}\eta_{i\sigma}\right]}{\sum_k \lambda_k|\eta_{k\sigma}(\mathbf{r})|^2}\Bigg|_{\mathbf{s}=0}. \end{aligned} \tag{3.80}$$

Finally, taking the limit $\mathbf{s}=0$, and expressing all in terms of $\mathbf{r}_2=\mathbf{r}$, it is possible to show that the delocalization field for this correlation correction is given by

$$D_\sigma(\mathbf{r}) = 2D^{HF}_\sigma(\mathbf{r}) + \frac{3!}{s^2}\left\langle \xi'_{2\sigma}(\mathbf{r},\mathbf{r})\right\rangle. \tag{3.81}$$

What Eq. (3.81) suggests is that increasing the complexity of the second-order RDM in terms of the first-order RDM may exclude the possibility of having a short range local scalar field that captures the Pauli principle. This conclusion raises because in Eq. (3.81) the field $D_\sigma(\mathbf{r})$ depends not only on the average position of electrons but in their distance s.

Chapter 4

Results and discussion

4.1 Computational methods

For the GSIPT, we have performed the calculations using DFT in the Kohn-Sham formalism. In order to include the long-range behavior of the exchange potential and, therefore, better values of the KS energies, we employed the $\omega B97x$d exchange-correlation functional. The functional $\omega B97x$d is a hybrid functional that belongs to the family of the long-range corrected functionals [16]. This kind of functionals have the peculiarity that the Coulomb interaction that appears in the exchange density is split into two terms, that is:

$$\frac{1}{|\mathbf{r}-\mathbf{r}'|} = \frac{f(\mu|\mathbf{r}-\mathbf{r}'|)}{|\mathbf{r}-\mathbf{r}'|} + \frac{1-f(\mu|\mathbf{r}-\mathbf{r}'|)}{|\mathbf{r}-\mathbf{r}'|} \tag{4.1}$$

where f is a function that must fulfill $f(\mu x \to 0) = 1$ and $f(\mu x \to \infty) = 0$. Thus, the first term of the RHS of (4.1) accounts for the short-range (SR) interactions, while the second term accounts for the long-range (LR) interactions. The general form of the long-range corrected functionals is

$$E_{xc} = E_x^{SR-DFT} + E_x^{LR-HF} + E_c^{DFT}, \tag{4.2}$$

where the superscript DFT, in the exchange and correlation parts of E_{xc} (first and third terms), means that in these terms a standard density functional approximation is used, such as local density approximation (LDA) or generalized gradient approximation. The second term of E_{xc} corresponds to the HF-type exchange with the long-range Coulomb interaction. This part gives the hybrid character to this functional. The basis set employed to expand the KS orbitals is the 6-311G + +(d, p), i.e., a *triple-zeta split-valence* with diffused and polarized Gaussian functions [33]. In this basis set, each atomic orbital of the atomic cores is written as a linear combination of six primitive Gaussian functions, while for each valence electron, three basis functions are used, where the first one is a linear combination of three primitive Gaussians and the other two are single Gaussians. The ++ symbol means that diffuse functions have also been included in all atoms: one s and three p diffuse functions per each non-hydrogen atom (carbons, oxygen, and nitrogen), and one s diffuse function per each hydrogen. Diffuse functions are primitive Gaussian functions with a small ξ exponent, used to capture electron density far from the nuclei. They are necessary for an accurate description of

inter and intramolecular interactions (H-bond) and excited state densities. The symbol (d, p) means that polarization functions are used in all the atoms. Polarized functions are primitive Gaussians with high angular momentum. In particular, six d orbitals on non-hydrogen atoms and three p orbitals on hydrogens has been added. Polarized functions allows to describe the deformation of the electronic density caused by the induced polarization when an atoms approaches to form a molecule. Thus, polarization functions are essential for the theoretical description of chemical reactions [33].

4.2 Intramolecular proton transfer in the ground state

The degree of freedom used in the relaxed scan is the oxygen-hydrogen internuclear distance. We assume that the proton transfer process occurs only via the evolution of this coordinate. However, from Figure 4.1, it is seen that, at the beginning of the process, there is a difference between the curve associated to the relaxed scan with the curve associated to the *intrinsic reaction coordinate* (IRC). The IRC corresponds to the minimum energy path that follows the mass-weighted coordinates (normal coordinates) of the molecule in the chemical process along the PES [41]. The IRC is an idealization of the path that a reaction follows and, in every point, the atoms carry no kinetic energy. It usually gives the best agreement of reaction rates with experiments because it is the average path that atoms follow in a reaction where atoms move to moderate speed (temperature of few thousands of K). The difference with a relaxed scan is that the IRC takes into account contributions from degrees of freedom different from the $O-H$ distance. For instance, in our case, the IRC reveals that $C1-C7-N$ angle contributes to the reaction path. Hence, a relaxed scan is an approximation to the IRC as it can be seen in Figure 4.1. The IRC reveals that the CCN angle slightly decreases before the proton transfer and increases at the end of the reaction as is shown in Figure 4.2. Overall, the relaxed scan is a good approximation to the IRC of a proton transfer. The reason we used relaxed scan is that in excited states we do not have the machinery to compute IRC's but relaxed scans only.

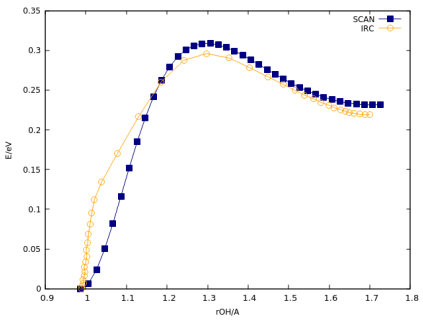

Figure 4.1: Comparison between relaxed scan along $O-H$ internuclear distance and IRC.

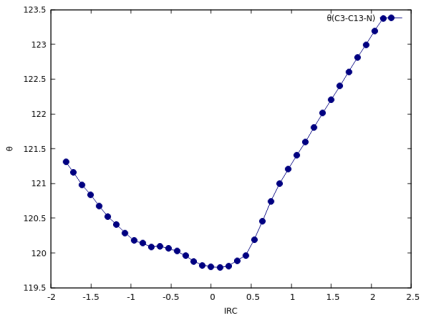

Figure 4.2: Variation of the $C1-C7-N$ angle in the proton transfer.

Fortunately, in the neighborhood of the maximum of the scan, both curves differ in less than $0.02\mathrm{e}V$, and it is in this region where rupture and formation of chemical bond occur.

Thus, with the purpose of studying changes in the chemical bonds in the proton transfer process, the scan procedure is a good approximation and, therefore, we assume from now on that the PES for the process is faithfully represented by a relaxed scan. We use very fine spacing between points along the scan (0.02Å).

4.2.1 Electron localization function along the reaction path in the ground state

Figure 4.3 depicts the PES for $S0$ with the localization domains for an isovalue of the ELF equals to 0.8 for four molecular structures of interest. The first corresponds to the Enol structure, whose $O-H$ internuclear distance is 0.98Å. In this structure, it is possible to observe that there is a localization domain that involves both oxygen and hydrogen atoms, which accounts for the fact that in this initial structure there is a covalent chemical bond between these both atoms. The structure located at the end of the curve, at 1.70Å, corresponds to the Keto form, which is the product of the chemical reaction. The isosurface shows clearly that there is a covalent bond between the hydrogen and the nitrogen. The structure located at 1.28Å corresponds to the transition state of the reaction. In this case, the oxygen and the hydrogen atoms belong to two different localization domains. On the other hand, at this point, the hydrogen and the nitrogen atoms belong to the same localization domain, which indicates that the bifurcation point between $V(H)$ and $V(N)$ is higher than 0.8 (it is close to 0.9), and hence, the hydrogen is more correlated with the nitrogen than with the oxygen. However, this does not imply that there is a covalent bond between the hydrogen and the nitrogen: as we will see in Section 4.2.1, at the TS, the hydrogen atom behaves as an independent entity, because it contains its own attractor. Finally, the structure located at 1.20Å is associated to another kind of transition state which we call the *electronic-transition state* (elec-TS). The elec-TS corresponds to the point of the PES at which the correlations between the hydrogen and the oxygen and between the hydrogen and the nitrogen are equal.

4.2.2 Electronic populations, attractors and catastrophes

Several catastrophes in the topology of ELF occurs as the proton transfers proceeds. These catastrophes define different bonding states along the reaction and are easily identified as discontinuities in the average number of electrons of the basins along the reaction coordinate, as it is depicted in Figure 4.4. From this, it is possible to identify the points along the reaction coordinate at which catastrophes occurs. Particularly, these bifurcation catastrophes are related with the rupture and formation of chemical bonds: they correspond to points in which a certain basin disappears giving origin to new ones. Thus, at $r_{OH} = 1.12$Å the disynaptic basin $V(O,H)$ disappears at the same time that two new basins appear, namely $V(O)$ and $V(H)$, representing the rupture of the hydroxyl $(O-H)$ bond. Next, at $r_{OH} = 1.42$Å the monosynaptic basins $V(H)$ and $V(N)$ merge, giving origin to the disynaptic basin $V(N,H)$. The latter represents the formation of the covalent bond between hydrogen and nitrogen $(N-H$ bond). Note that in the Enol form, the electronic population of $V(N)$ is 2.65 electrons, which decreases until a minimum value of 2.21 at $r_{OH} = 1.40$Å, where the bonding

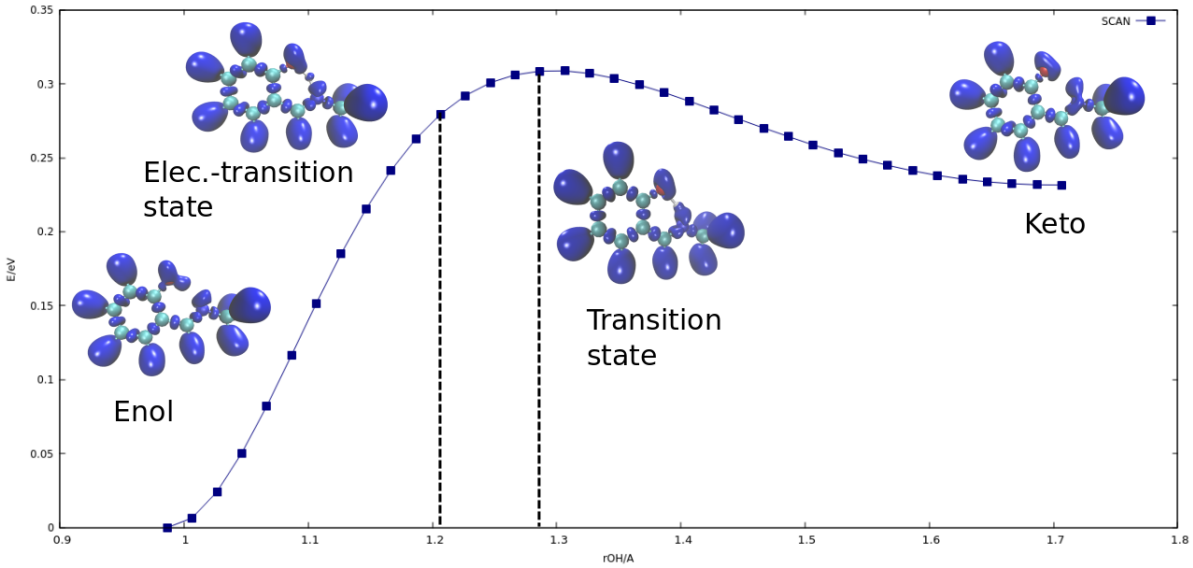

Figure 4.3: Variation of the molecular energy (in eV) with the elongation of the $O-H$ internuclear distance (in Å) in the ground state. Also localization domains for four molecular structures in the proton transfer are shown. Vertical dashed lines indicates the energies of the electronic TS and the thermodynamic TS.

of hydrogen and nitrogen atom occurs. Then, once formed the $V(N,H)$ basin, its electronic population decreases from 2.66 to 2.28 electrons until its minimum in the Keto form.

An important feature is the existence of a hydrogen monosynaptic basin in the region between 1.12Å and 1.40Å. This is the principal evidence that proton transfer occurs via a pseudoatomic form of the proton, and that, the rupture of the $O-H$ bond and the formation of the $N-H$ are not simultaneous. It is worth noting that the rupture of the $O-H$ bond occurs several points before the TS (located at $r_{OH} = 1.28$Å). From a chemical point of view, this indicates that the electronic processes involved in chemical reactions occur before the thermodynamical transition state. Also, at the TS, there are no appreciable changes in the basins: all significant changes in the process occur before or after thermodynamic TS.

At the beginning of the reaction, there are two monosynaptic basins associated with the oxygen atom whose populations have been added (in Figure 4.7, two spheres in purple over the oxygen atom in red which represent the $V(O)$ basins). These basins have electronic populations of 2.08 and 2.22 (4.29), and they correspond to the two non-bonding electron pairs of this atom. In Figure 4.4, these basins corresponds to the $V(O2)$. Also, after rupture of $O-H$ bond, a new monosynaptic basin appears, which is associated to the oxygen ($V(O1)$) that carries part of the electronic population that belonged to the hydroxyl bond ($O-H$). At 1.10Å the electronic population of $V(O,H)$ basin is 1.85 electrons. At the next step in the scan, the electronic population of $V(O1)$ is 1.40 while the $V(H)$ is 0.45. Hence, the rupture of the hydroxyl bond is asymmetric in the sense that most of the electronic population is carried away by the oxygen atom (due to the electronegativity of the oxygen atom). Once the $V(H)$ basin is formed, its electronic population begins to descend until a minimum of 0.35 electrons at 1.20Å. Then its population increases until it reaches a population of 0.49 electrons. Thus, the process does not correspond to a transference of a bare proton, but a

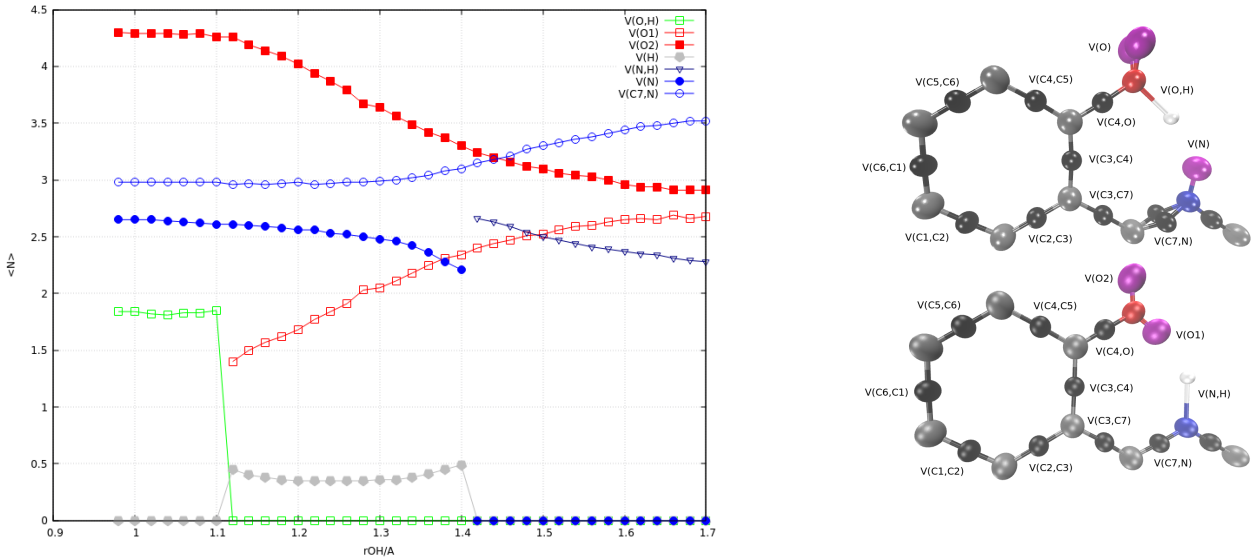

Figure 4.4: Electronic populations of the basins involved in the proton transfer process.

partially screened proton. It is important to note that the minimum of $\langle N(V(H))\rangle$ is located in the neighborhood of the TS (precisely between the elec-TS to the TS).

As the reaction progresses, the electronic population of the $V(O1)$ increases at the same time that the electronic population of $V(O2)$ decreases. This can be explained in terms of the electronic fluctuation between both $V(O1)$ and $V(O2)$ basins: these basins are more correlated in the Keto form than in the Enol. Interestingly the total electronic population of the oxygen at the end of the reaction (in the Keto structure) is 5.59 electrons, which is quite high compared with the classical structures (Lewis) predicted by the organic chemistry rules: for an oxygen atom in an organic molecule like SMA, it is expected its electronic population to be close to 4 electrons, corresponding to the two non-bonding electron pairs. This unusual highly charged O atom (almost 3 non-bonding pairs) would partially explain why the barrier for the proton transfer in the ground state is high compared with the proton transfer in the excited state in which there is no barrier. The Coulomb repulsion among these three pairs of electrons that build up along with the proton transfer can be postulated as the main physical reason for the high barrier in the ground state.

Figure 4.5, shows the variation of electronic populations of the basins of the aromatic ring (six-carbon ring). Note that the electronic population of the basins close to the oxygen atom, namely, $V(C3, C4)$ and $V(C4, C5)$, decreases from 2.78 to 2.49 and from 2.76 to 2.47, in the course of the reaction, respectively. Similarly, the electronic population of the $V(C2, C3)$ basin also decreases. However, the reduction of the population of $V(C2, C3)$ is more abrupt: at 1.50Å, its electronic population decreases from 2.71 to 2.50, which is compensated with the increase of the electronic population of the basin $V(C3, C7)$ in a similar amount (from 2.65 to 2.68). This spreading of the population of the bonds in the aromatic ring points in the direction of the idea the high barrier and the endothermicity of the reaction in the ground

state are associated to a loss of *aromaticity* of the ring, which entails an increase of the total energy of the molecule. The loose of aromaticity (electron delocalization) is an argument that has been previously used by Rocha et al. [25] to explain the barrier in the ground state and the lack of it in the excited state.

In the context of topological analysis of electronic localization, we define the *population spreading*, σ (spreading index), as the diference of electronic population between the basin with greater electronic population and the basin with the lower electronic population in the Keto structure, minus the same quantity in the Enol structure i.e.,

$$\sigma = (\langle N \rangle_{max} - \langle N \rangle_{min})_{Keto} - (\langle N \rangle_{max} - \langle N \rangle_{min})_{Enol} \,. \tag{4.3}$$

For the GSIPT, the basin of the aromatic ring with the higher electronic population is the $V(C5, C6)$ (in brown), while the basin with the lower one is the $V(C6, C1)$ (navy blue). Here, the σ index has a value of 0.51, which we should compare with the σ index for the ESIPT.

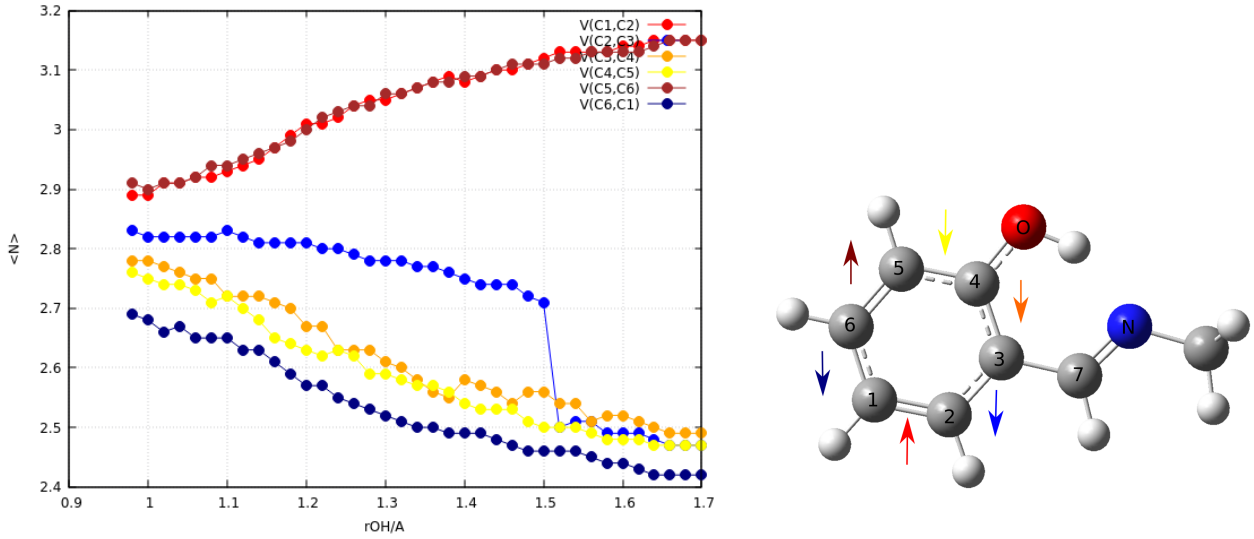

Figure 4.5: Variation of elec. populations of basins of the aromatic ring along GSIPT.

On the other hand, the basins associated to the functional groups adjacent to the ring increase its electronic population along the process (see Figure 4.6). These basins are $V(C4, O)$, $V(C3, C7)$ and $V(C7, N)$, whose increments are from 1.59 to 1.99, from 2.31 to 2.96 and from 2.98 to 3.52 electrons respectively. Thus, there is an electronic flux from the aromatic ring to the functional groups, as a consequence of the high electronegativity (capacity of an atom in a molecule to attract electrons) of the oxygen and the nitrogen.

In order to complete the scheme of the proton transfer in the ground state, it is important to identify the positions of the attractors in the SMA molecule. Once known these positions, we can determine the points along the reaction in which catastrophes occur. Figures 4.7 to 4.12 show the attractors for these key points in the reaction path. In these figures, gray

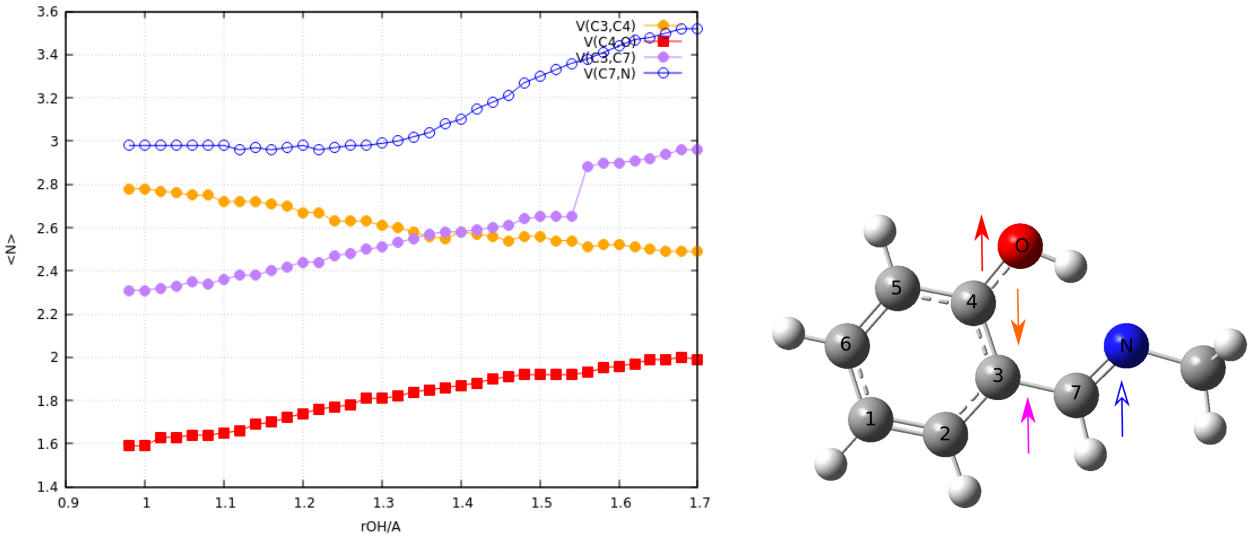

Figure 4.6: Variation of elec. populations of basins of the functional groups adjacent to the aromatic ring along GSIPT.

spheres corresponds to the attractors of the core basins of carbons $C(C)$, black spheres represent the location of the attractors associated to the disynaptic basins $V(C_i, C_j)$, $V(C, O)$ or $V(C, N)$, purple spheres are the attractors associated to the valence monosynaptic basins $V(O1)$, $V(O2)$ and $V(N)$ (non-bonding electron pairs), and the red and blue spheres corresponds to the attractors of the basins $C(O)$ and $C(N)$ respectively. Finally, a white sphere is used to represent the attractor associated to the $V(O, H)$ basin in the first step of the reaction, the $V(H)$ in the intermediate region, or the $V(N, H)$ basin in the Keto form. The numbers over the spheres correspond to the electronic populations of the corresponding basins. The first diagram (Figure 4.7) corresponds to the Enol structure. In this diagram, it is possible to identify two attractors over the oxygen atom corresponding to the two non-bonding electron pairs with electronic populations of 2.08 and 2.22. Also, we can recognize the double bond between the nitrogen and the adjacent carbon: this corresponds to the two attractors (black spheres) located between these atoms, whose populations are 1.43 and 1.55. In the second diagram (Figure 4.8) the attractors at $r_{OH} = 1.02$Å are shown. At this point the first catastrophe takes place, that is, the two attractors corresponding to the non-bonding electron pairs of the oxygen are merged in only one attractor with an electronic population of 4.29. Figure 4.9 shows the attractors at the point where the rupture of the $O - H$ bond occurs. In fact, at this point, two new attractors appears corresponding to the $V(O1)$ and the $V(H)$ basins. Then, at $r_{OH} = 1.16$Å two attractors of the $V(C, N)$ merge, but this does not represent a physical catastrophe because the population of the new basin after the catastrophe (2.96 electrons) is equal to the sum of the populations of the basins before the catastrophe, and hence, the chemical character of this bond does not change. Next, several points later, at $r_{OH} = 1.42$Å, it appears an attractor associated to the $V(N, H)$ basin with an electronic population of 2.66. Finally, Figure 4.12 shows the attractors of the Keto form. The geometrical disposition of the attractors of the Keto form is quite similar of the attractors showed in the Figure 4.11, with the only difference in the orientation of the attractor of the

$V(N, H)$ basin.

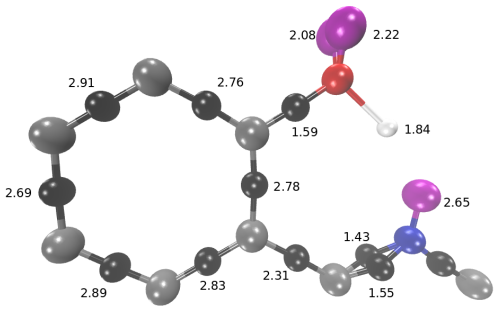

Figure 4.7: Attractors of the Enol structure. $r_{OH} = 0.98$Å.

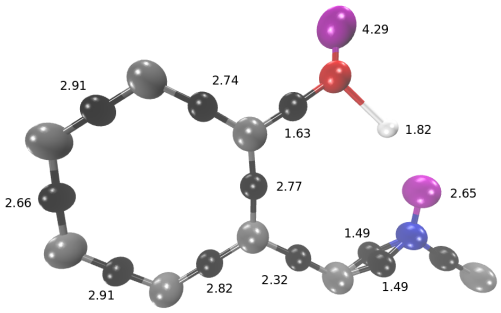

Figure 4.8: Attractors at $r_{OH} = 1.02$Å.

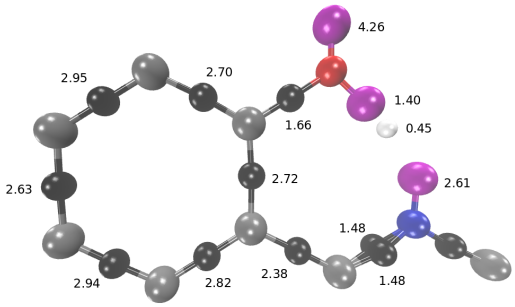

Figure 4.9: Attractors at $r_{OH} = 1.12$Å.

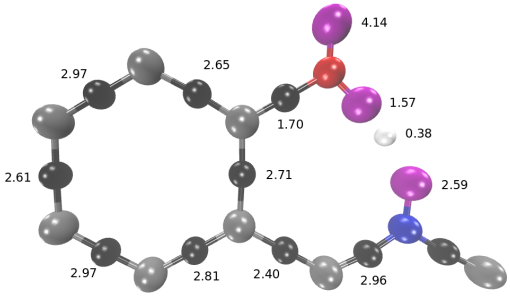

Figure 4.10: Attractors at $r_{OH} = 1.16$Å.

4.2.3 Electronic fluctuacions and bifurcation points

Covariances of electronic population between basins in the intermediate region of the GSIPT (between 1.12Å and 1.40Å) are shown in the Figure 4.13. We see that, as the reaction progresses, the covariances between $V(H)$ and $V(O)$ increases (red curve) because the second term of $\langle cov\,(V(H), V(O))\rangle$ in the Equation (2.32) (which corresponds to the integration of the second-order RDM) becomes less important. Hence, the electronic fluctuations, and also, the correlations between these basins, decrease with the proton transfer. On the other hand, the covariances between $V(H)$ and $V(N)$ decreases (blue curve) as a consequence of the increasing of the correlated term of $\langle cov\,(V(H), V(N))\rangle$. Thus, the electronic fluctuation between $V(H)$ and $V(N)$ increases in the process.

The elec-TS allows characterizing the reaction from the electronics instead of thermodynamics. We define this point of the process formally in terms of the covariances. Elec-TS is defined as the point in the PES in which the covariances between the basin associated to

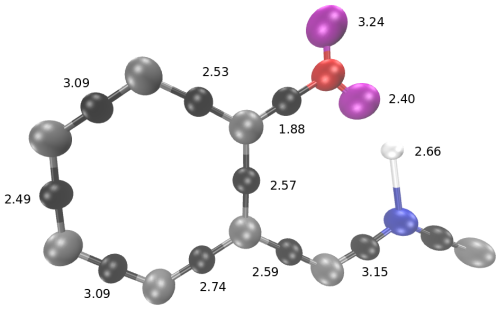

Figure 4.11: Attractors at $r_{OH} = 1.42$Å.

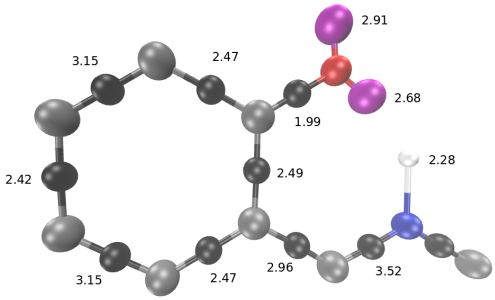

Figure 4.12: Attractors of the Keto structure. $r_{OH} = 1.70$Å.

the proton, $V(H)$, and the basin of the donor atom, $V(O)$, is the same than the covariances between $V(H)$ and the basin associated to the acceptor atom, $V(N)$. This means that, at this point, electrons belonging to $V(H)$ are as correlated with $V(O)$ as with $V(N)$. From Figure 4.13 we can notice that such point corresponding to the elec-TS is located between 1.18Å and 1.20Å.

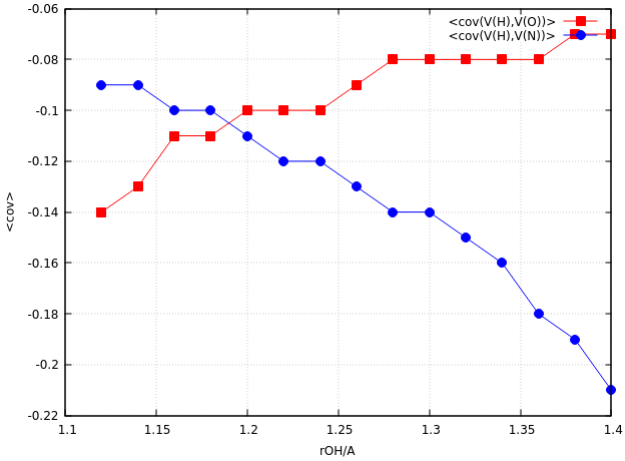

Figure 4.13: Electronic fluctuations in the intermediate region of the proton transfer.

It is important to emphasize that the covariances showed in Figure 4.13 correspond to the KS because since in the calculation of these quantities, we use the KS orbitals to expand the electronic density as the second-order RDM. Despite ρ_2 of the KS system is different than that the real system, it gives the correct tendencies. (In fact, in DFT we cannot know the exact form of ρ_2 in real systems, but only the adiabatic average of the exchange-correlation density). The precision with which we determine the position of the elec-TS is limited by the spacing between the points of the relaxed scan (in this case is of 0.02Å). Thus, a finer relaxed scan would give us a more precise location of the elec-TS, but such degree of accuracy is chemically not very relevant.

Another descriptor for the electronic fluctuations between basins is the bifurcation point between them: the smaller the ELF at the bifurcation point of two basins, the less per-

sistent the topology of these basins and the higher the electron fluctuation (delocalization) between them [3]. Bifurcation points between the basins $V(H)$ and $V(O)$ ($\eta\left(V(H), V(O)\right)$, red curve), and between $V(H)$ and $V(N)$ ($\eta\left(V(H), V(N)\right)$, blue curve) are shown in Figure 4.14. Notice that the tendencies of the bifurcation points are opposite to those obtained with the covariances, that is, while the higher the bifurcation points between two basins are, the more correlated are these basins. The elec-TS can also be defined as the point in the PES in which the value of ELF at the bifurcation points of $V(H)$ and $V(O)$ and $V(H)$ and $V(N)$ is the same. Additionally, because variations of the bifurcation points are smoother than the variations of the covariances, we have a better precision for the location of the elec-TS. According to the point in which the two curves intersects, the elec-TS is located at $r_{OH} = 1.20$Å.

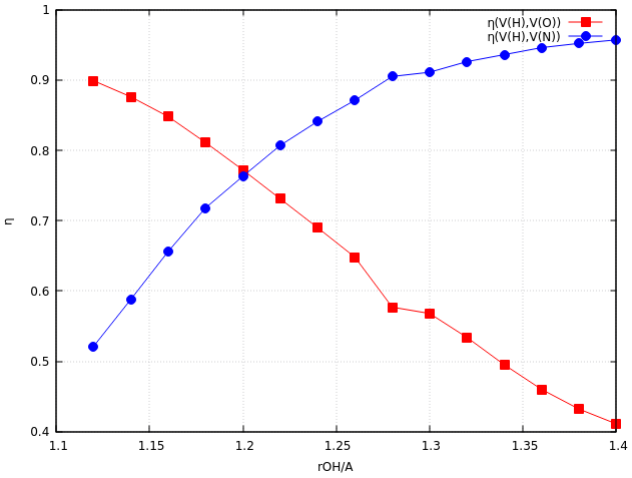

Figure 4.14: Bifurcation points of $V(H)$ and $V(N)$ and $V(O)$ basin in the intermediate region of the proton transfer.

4.3 Intramolecular proton transfer in the excited state

A remarkable difference between the proton transfer in the first singlet excited state (S_1) compared with the ground state is that, in the excited state, there is no energetic barrier between the Enol and Keto forms. So, once reached the excited state through absorption of radiation, the molecule carries out the proton transfer spontaneously. The reason for this behavior is that there is no local minimum in the PES for S_1 close to the structure of the Enol (Frank-Condon state), and hence, this molecular form is not stable in the excited state. In fact, only the Keto form is stable in the excited state, which has a local minimum located at the geometry of this molecular form. Thus, the ESIPT process consists of the transit of the system from an unstable molecular structure to a stable one. The excitation energies of the molecule along the ESIPT calculated with the level of theory described in Section (4.1) are shown in Figure 4.15. The excitation energy of the Enol form is 3.94eV, which is a good prediction of the TD-DFT, considering that the experimental value is 3.97eV [23]. This excitation energy corresponds to a wavelength of 315nm, while the excitation energy for the Keto form calculated with the same level of theory is of 3.01eV, which corresponds

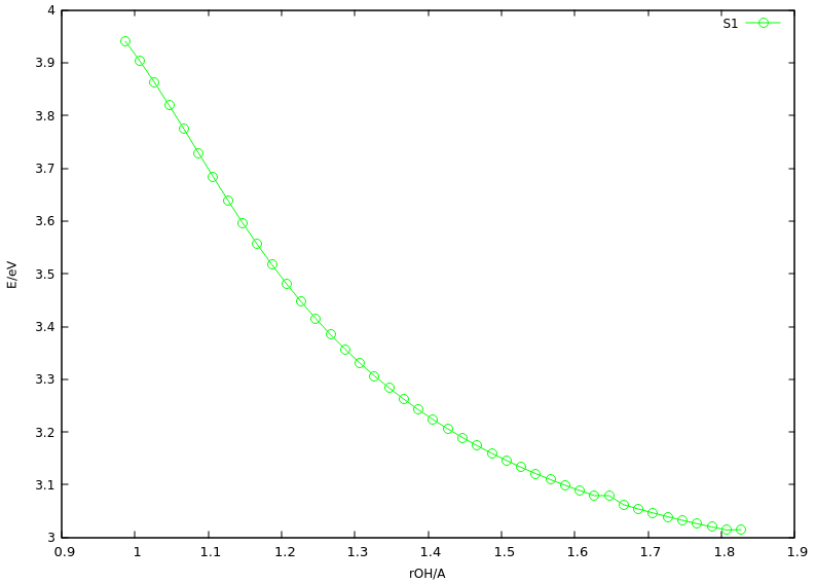

Figure 4.15: Excitation energies along ESIPT

to a $411nm$. So, the molecule suffers a redshift after proton transfer, from the UV region to the visible region of the spectrum. This large redshift and the ultrafast proton transfer is what makes this molecule interesting for molecular photoswitches.

The relative energies of the PES for the ESIPT normalized to the energies of the Enol form in $S0$ are depicted in Figure 4.16. The energies of the PES of $S1$ are obtained through a relaxed scan in which we have added, to each point of the relaxed scan in $S0$, the excitation energies. Also, in this procedure, we impose the constraint to block the dihedral angle formed between the atoms $C4$-$C3$-$C7$-N. This constraint prevents that the system in the excited state returns to the ground state via a transition through a conical intersection that connects both electronic states.

One would expect that, after normalizing the energies of $S1$ to the energy of the Enol form in $S0$, these coincide with the excitation energies. However, the energies of the proton transfer in $S1$ are slightly higher than the excitation energies. The reason is that blocking the dihedral angle leads to slightly higher energies than those of the actual reaction path in $S0$. So, the first point of the PES in $S1$ has an energy of $4.16eV$. Also, it is possible to see an additional point located just over the first point of the PES in $S1$, which has an energy of $4.42eV$. This point corresponds to the energy of the Franck-Condon (FC) structure, that is, the energy of the Enol form in the excited state with exactly the same optimized geometry as the Enol in $S0$ (vertical excitation). The first point of the PES is obtained after a geometrical optimization of all degree of freedom except for the OH distance; hence, it has lower energy than the FC. Hereafter, we call this point the *pseudo-FC*. Note that in the relaxing of the atoms when passing from the FC to the pseudo-FC, the oxygen-hydrogen internuclear distance has remained constant. All plots of the electronic populations in $S1$ begin at such point.

The localization domains of the ELF for an isovalue of 0.8, for the FC, the Keto form and the elec-TS structure, are also shown in Figure 4.16. Qualitatively, there are no appreciable

differences between the localization domains between both $S0$ and $S1$, which does not mean that there are no quantitative differences (electronic populations and covariances).

In the excited state, the elec-TS is located between $r_{OH} = 1.14$Å and $r_{OH} = 1.16$Å while, for the GSIPT, the elec-TS is located at $r_{OH} = 1.20$Å. The reason for such difference is that in the excited state the basic character of the nitrogen atom (the capacity to attract the hydrogen) is enhanced. Also, it should be noted that, in the ground state, the Keto form has a $O-H$ internuclear distance of 1.72Å, while in the excited state, the Keto form is located at $r_{OH} = 1.82$Å. Thus, the trajectory that connects the Enol and Keto forms in $S1$ is slightly longer than the same trajectory in $S0$.

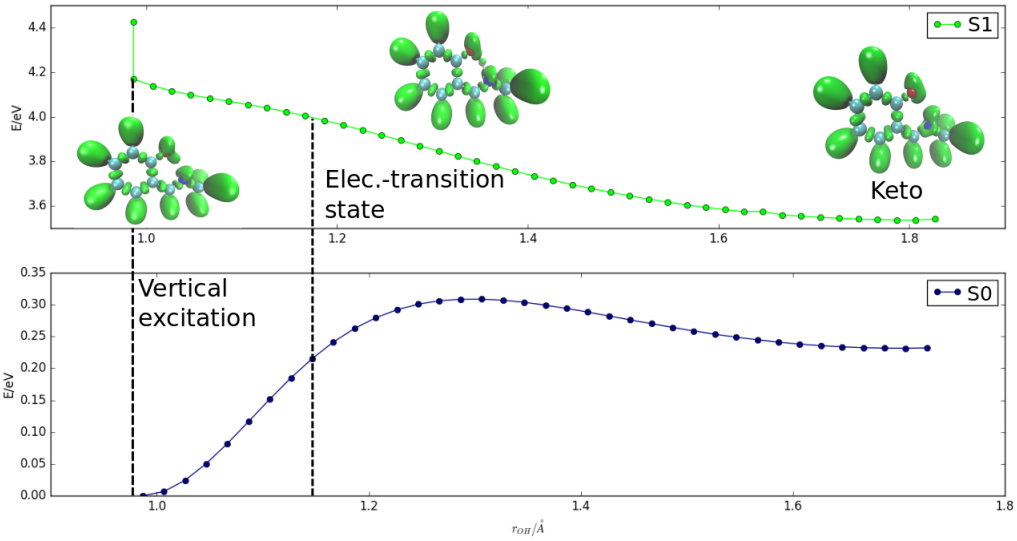

Figure 4.16: Comparison between the proton transfer in both $S0$ and $S1$ states. Also, localization domains for the FC, the elec-TS and the Keto structures are shown. Vertical dashed lines indicate the vertical excitation and the position of the electronic TS.

4.3.1 Electronic populations, attractors and catastrophes

Despite variations of electronic populations of basins in both $S0$ and $S1$, they seem qualitatively similar, but there are several quantitative differences. First, the detachment of the hydrogen atom of the oxygen occurs quite early compared with the proton transfer in $S0$: while in the ground state this catastrophe occurs at $r_{OH} = 1.12$Å, in the excited it state occurs at $r_{OH} = 1.06$Å. This can be explained by the enhanced ability of nitrogen to attract the hydrogen atom in the excited state. While in the Enol form of the GS the nitrogen has a usual pair of lone electrons, in the FC it has 3 non-bonding electrons. Besides, this "excess" of charge persists for a good part of the reaction path until just before the hydrogen bonds to the nitrogen (1.26Å). The strong electrostatic attraction between the positively charged hydrogen and the nitrogen is the driving force for the ultrafast proton transfer.

The domain of the proton transfer in which the hydrogen atom exists as an independent

entity is from $r_{OH} = 1.06$Å to $r_{OH} = 1.38$Å, which corresponds to 17 points in the relaxed scan, while in $S0$ this domain goes from $r_{OH} = 1.12$Å to $r_{OH} = 1.40$Å (15 points in the relaxed scan). The electronic population of $V(H)$ at $r_{OH} = 1.06$Å is of 0.43, reaching a minimum of 0.35 at the position of the elec-TS of $S1$, i.e., at $r_{OH} = 1.14$Å. In this part of the reaction, the hydrogen atom, which has a positive charge of 0.65e, feels a great electrostatic attraction to the nitrogen, due to the three non-bonding electrons located in the valence of this atom. Thus, the main argument that would explain that the proton transfer in the excited state occurs without an energetic barrier is that there is a driven force produced by the excess of negative charge on the nitrogen atom. Then, as the hydrogen atom approaches to the nitrogen, its population increases reaching a value of 0.55 at $r_{OH} = 1.38$Å, where the electronic population of $V(N)$ is of 2.77. The next point in the relaxed scan corresponds to the catastrophe in which the basins $V(H)$ and $V(N)$ merge giving rise to the $V(N, H)$, whose population is 3.33. This population keeps constant until $r_{OH} = 1.52$Å. After this point, a new catastrophe occurs which was not present in the GSIPT. This catastrophe consists in the formation of two monosynaptic basins associated to the nitrogen, with populations of 0.48, causing an abrupt decrease in the electronic population of $V(N)$ basin from 3.29 to 2.37. This suggests that part of the electron density located in the $N - H$ bond is displaced symmetrically to both sides of the molecular plane, forming these basins. A chemical picture consistent with the topology of ELF in the Keto isomer is that of the nitrogen atom having a radical (unpaired) electron.

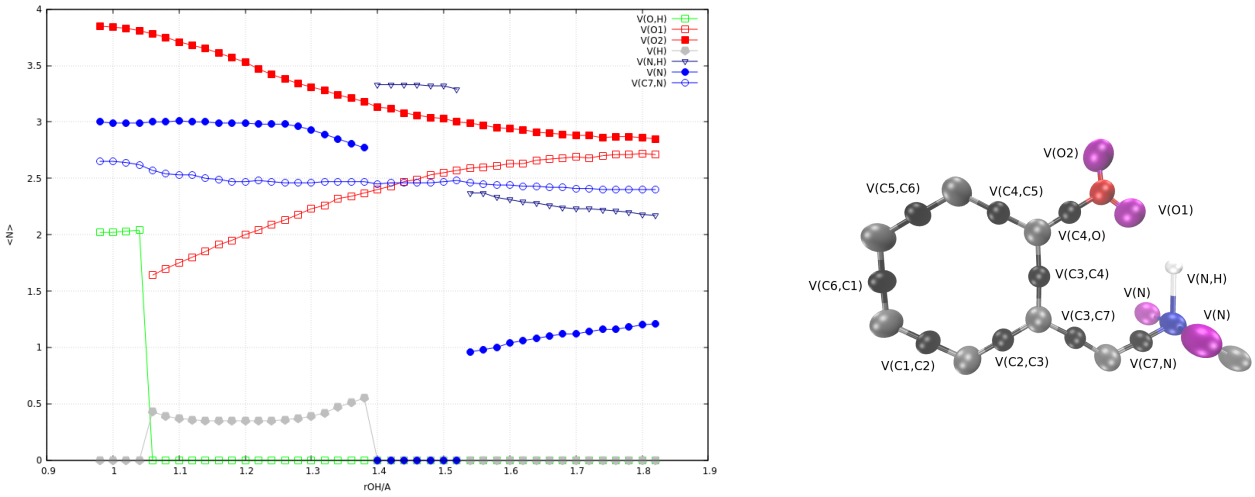

Figure 4.17: Electronic populations of the basins involved in the proton transfer reaction in the first excited state.

At the pseudo-FC, there is only one monosynaptic basin associated with the oxygen atom ($V(O2)$), with a population of 3.92. Also, the population of the $V(O, H)$ basin is of 1.97, which increases slightly until 2.04 at $r_{OH} = 1.04$Å. At the next step, the $V(O, H)$ basin is split in the basins $V(H)$ and $V(O1)$, where the electronic population of this latter is of 1.64, while in $S0$ is of 1.40. Then, it is observed the same behavior in the basins of the oxygen atom which was observed in the GSIPT: as the population of $V(O2)$ decreases, the population of $V(O1)$ increases.

Another important difference between the GSIPT and ESIPT is observed in the behavior of the $V(C7, N)$ basin (see Figure 4.19). In $S0$ this basin appears in the Enol form with an electronic population of 2.98 and then increases with the evolution of the process until reaching its maximum value of 3.52 at the Keto form, implying the strengthening of this double bond. On the other hand, in $S1$, the $V(C7, N)$ basin appears with an electronic population of 2.81 which decreases reaching its minimum at the Keto form with a value of 2.40. Hence, this suggests that in the excited state, the bond between nitrogen and the carbon atom gets weak, which allows the increasing of the population on the nitrogen and, hence, improving its basic character.

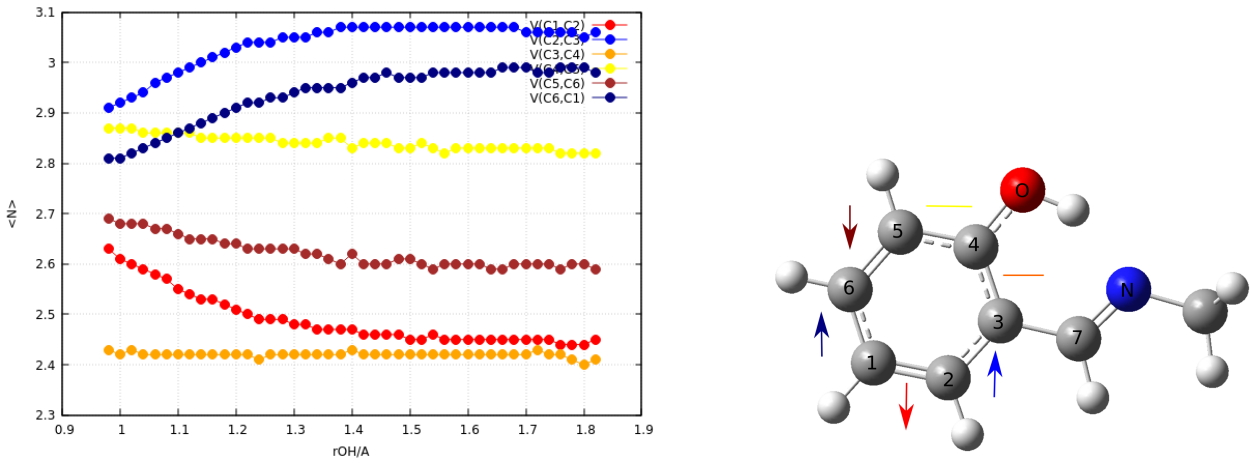

Figure 4.18: Variation of elec. population of basins of the aromatic ring along ESIPT.

The electronic populations of basins belonged to the aromatic ring are shown in Figure 4.18. Unlike GSIPT, in which the basins adjacent to the functional groups, namely, $V(C3, C4)$ and $V(C4, C5)$ decreases its electronic populations, in the ESIPT the electronic populations of these basins remain practically constant, with values around of 2.42 and 2.87. Also, the behavior of the basins $V(C1, C2)$, $V(C2, C3)$, $V(C5, C6)$ and $V(C6, C1)$ are in the opposite direction to the variations of the same basins in $S0$. For example, the variation of $V(C2, C3)$ basin is from 2.91 at the pseudo-FC to 3.06 at the Keto form, while in $S0$, this variation goes from 2.83 at the Enol to 2.47 at the Keto form.

In the same way that in the GSIPT, there is a population spreading in the aromatic ring. In the ESIPT, the basin with higher electronic population is the $V(C2, C3)$ (light blue), while the basin with the lower one is the $V(C3, C4)$ (orange). Thus, the σ index in the ESIPT has a value of 0.47. While it is true that this value is lower than the spreading index of the GSIPT, the difference is actually small, and it is not possible to identify any difference in the loss of aromaticity between both GSIPT and ESIPT with this index.

The variations of populations of the basins corresponding to the groups adjacent to the aromatic ring are shown in Figure 4.19. The carbonyl bond ($V(C, O)$) has an electronic population of 1.78 at the pseudo-FC, which reaches a value of 1.93 at the Keto form. This slight increase of the $C - O$ bond order is accompanied by a decreasing of the population of $V(O2)$ basin. Thus, the electron density flows from to the non-bonding electron pairs of

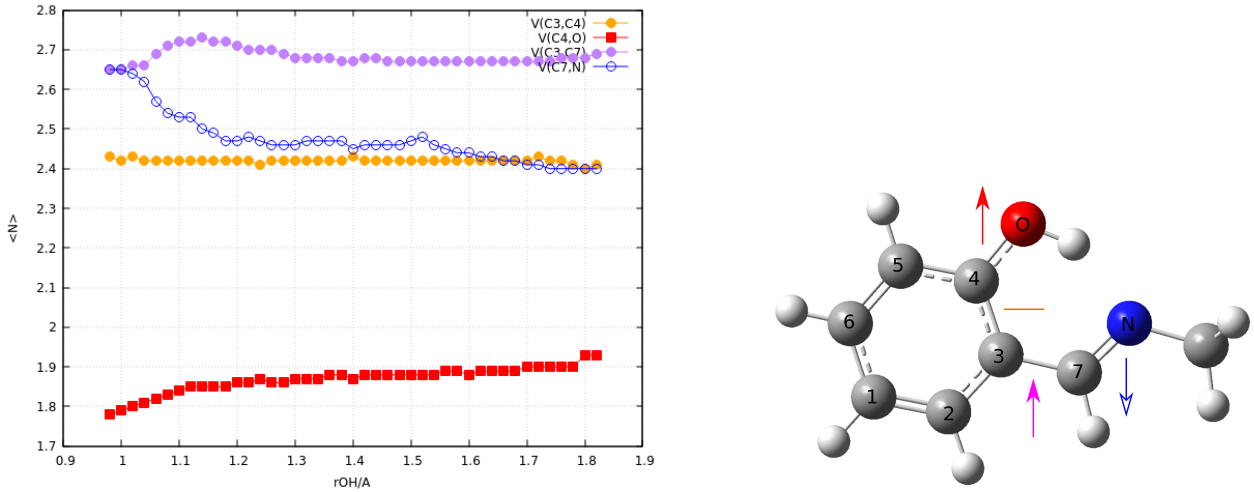

Figure 4.19: Variation of elec. populations of basins of the functional groups adjacent to the aromatic ring along ESIPT.

the oxygen to the covalent bond between the oxygen and the carbon. Both $V(C3, C7)$ and $V(C7, N)$, have an electronic population of 2.65 electrons in the pseudo-FC but its variations along the reaction path are different. While the basin $V(C7, N)$ decreases its electronic population, the behavior of the basin $V(C3, C7)$ is more complicated. At the beginning of the reaction, the electronic population of the $C3 - C7$ bond increases until a maximum value of 2.73, and then it slowly decreases until a constant value of 2.67. Curiously, the maximum value of $\langle N(V(C3, C7))\rangle$ appears at $r_{OH} = 1.14$Å, i.e., at the electronic transition state.

Attractors and catastrophes in $S1$ are shown in Figures 4.20 to 4.25. The catastrophes that occur in the ESIPT correspond to the rupture of the $O - H$ bond, the formation of the $N - H$ bond, and the appearance of the two symmetrical attractors of the nitrogen atom. Figure 4.20 shows the attractors of the FC structure. A remarkable difference with the Enol structure of $S0$ is the rearranging of the electrons along the functional groups. Thus, part of the 4.3 electrons in the $V(O)$ basin are redistributed between the adjacent bonds, increasing the populations of the $V(C, O)$ and the $V(O, H)$ basins, from 1.59 to 1.54 and from 1.84 to 1.97, respectively. Similarly, part of the electrons located in the $V(C7, N)$ basin (population equal to 2.98 in $S0$) migrates towards the valence of the nitrogen and the adjacent $C3 - C7$ bond. Thus, the electronic population of the non-bonding attractors of the nitrogen atom in the excited state with the same molecular geometry of the Enol of the ground state is of 2.90, which increases until 3.00 after the relaxing of the atoms, giving the structure of the pseudo-FC. The step that connects the FC with the pseudo-FC brings an increment of the population of the $V(O, H)$ basin from 1.97 to 2.02. An equalization of the populations of the basins $V(C3, C7)$ and $V(C7, N)$, having both 2.65 electrons, occurs too.

The catastrophe corresponding to the rupture of the $O - H$ bond is shown in Figure 4.22. There are several differences compared with the same catastrophe of the ground state proton transfer (Figure 4.9). First, while in $S0$, the $V(O2)$ has 4.26 electrons, in the excited state this basin has a population of 3.78. Also, the $V(O1)$ basin (which has an origin in

the breaking of the hydroxyl bond) has a population of 1.40 while in $S1$ it is 1.64 electrons. Note that the population of the $V(H)$ basin (0.43) only differs slightly with its equivalent of the $S0$ (0.45). Next, at $r_{OH} = 1.40$Å the catastrophe associated to the formation of the $N - H$ bond occurs (Figure 4.23). Compared with the same catastrophe in $S0$, it is noticed that the basins $V(C, O)$ and $V(O1)$ have the same electronic population in both states, 1.88 and 2.40, respectively. On the contrary, the electronic populations of the basins $V(N, H)$ and $V(C7, N)$ differ considerably. While in the ground state these have 2.66 and 3.15 electrons respectively, in the excited state they have 3.33 and 2.45, respectively. This excess of electronic density localized in the volume of the $V(N)$ would imply that this molecular structure is an unstable one. Therefore, in order to reach the minimum in the PES of the $S1$, the nitrogen atom must rearrange the excess of charge. Thus, at $r_{OH} = 1.54$Å, it appears two new attractors associated to the valence of the nitrogen, disposed symmetrically to both sides of the molecular plane (Figure 4.24). Finally, at $r_{OH} = 1.82$Å (Figure 4.25) the attractors of the Keto structure are shown. The fundamental difference with the Keto structure of the $S0$ is that, in the excited state, there are 1.21 electrons in excess over the nitrogen, which gives it a radical character.

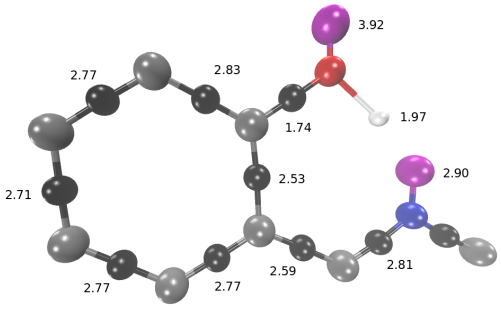

Figure 4.20: Attractors of the FC structure. $r_{OH} = 0.98$Å.

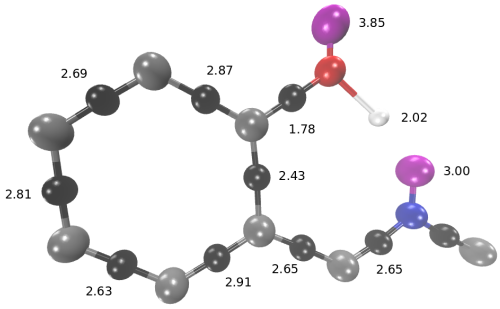

Figure 4.21: Attractors of the pseudo-FC. $r_{OH} = 0.98$Å.

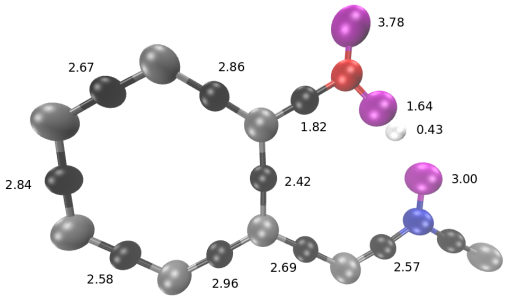

Figure 4.22: Attractors at $r_{OH} = 1.06$Å in $S1$.

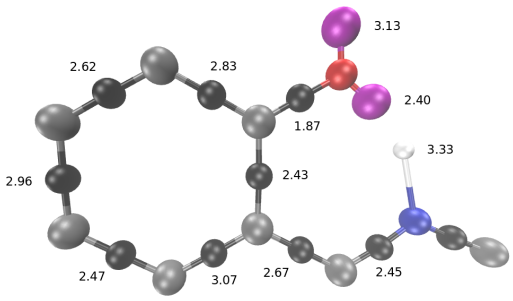

Figure 4.23: Attractors at $r_{OH} = 1.40$Å in $S1$.

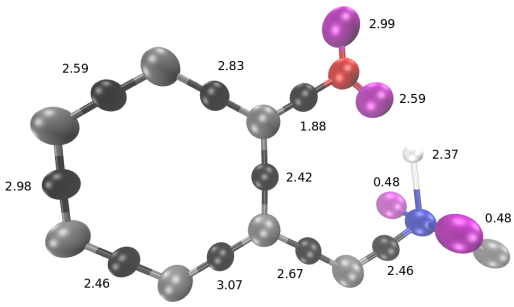

Figure 4.24: Attractors at $r_{OH} = 1.54$Å in $S1$.

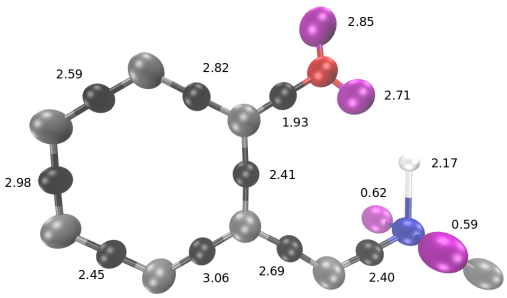

Figure 4.25: Attractors of the Keto structure of $S1$. $r_{OH} = 1.82$Å.

4.3.2 Electronic fluctuations and bifurcation points

The quality of the data depicted in Figure 4.26 is directly related to the degree of approximation used in the reconstruction of the second-order RDM. In this case, we have used the HF-like reconstruction of the $\rho_{2\sigma}$ (Eq. 3.60). Although it is true that this approximation is the simpler one, it comes with a relatively cheap computational cost. On the other hand, $\rho_{2\sigma}$ with the BB correlation correction gives better results for the covariances. However, the BB reconstruction for the $\rho_{2\sigma}$ fulfill neither the Pauli exclusion principle nor the cusp condition (Eqs. (3.61) and (3.62)), and hence, it cannot be used for the calculation of the ELF [5]. Figure 4.26 shows the electronic covariance between $V(H)$ and $V(O)$ and $V(N)$. A step of

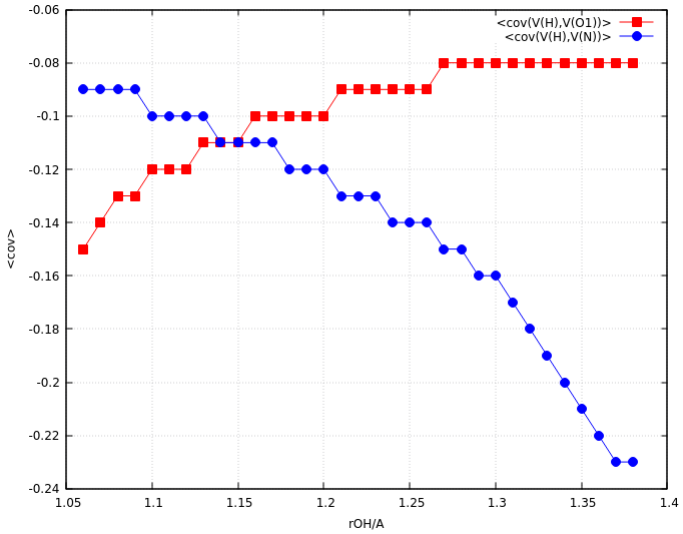

Figure 4.26: Electronic fluctuations in the intermediate region of the proton transfer.

0.01Å has been used to have more precision in the position of the elec-TS. The covariances show that the elec-TS is located between 1.14Å to 1.15Å with a value of -0.11 (the same value found in the elec-TS of the ground state). Moreover it is possible to note that the increase in the fluctuations between $V(H)$ and $V(N)$ (blue curve) is greater than the decrease

in the fluctuations between $V(H)$ and $V(O)$, possibly due to the high electronegativity of the oxygen atom.

Additionally, the delocalization between the basins $V(H)$ and $V(N)$, and between $V(H)$ and $V(O)$, could be understood in terms of its bifurcation points, which are shown in Figure 4.27. Following the rule that electronic TS corresponds to point where both bifurcation points are equal, then this is predicted to be located at 1.16Å, which agrees with the one estimated with the covariances. The value of ELF at the bifurcation point of the elec-TS is approximately 0.770. This high value of the bifurcation implies that the electrons are quite delocalized between these three atomic centers because the topology among them is not very persistent.

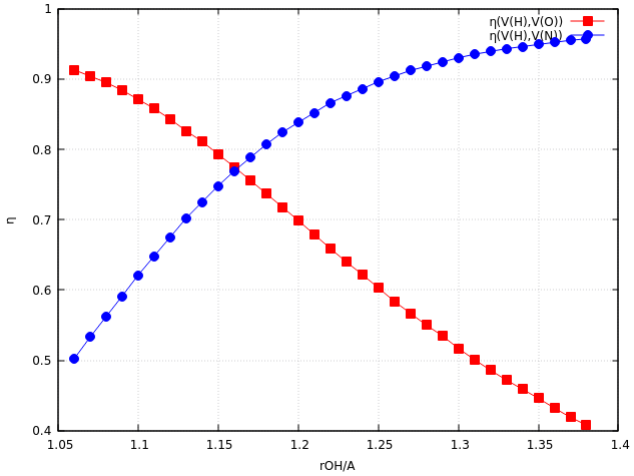

Figure 4.27: Bifurcation points between $V(H)$ and $V(O)$ and $V(N)$ basin in the intermediate region of the proton transfer in $S1$.

4.4 Comparison of the covariances between proton transfer in the ground and the excited state

There are certain differences between the evolution of the covariances between basins in both, GSIPT and ESIPT, as can be seen in the attractor diagrams. In Figures 4.28 to 4.35 the covariances between significant basins along the GSIPT are shown, namely, Enol, elec-TS, TS and Keto. Similar diagrams for the reaction in the excited state are shown in Figures 4.32 to 4.35 . The covariances that show higher changes are those located next to the oxygen, hydrogen and nitrogen atoms. For example, the covariance between the $V(O2)$ and the $V(C,O)$ basins in the Enol takes a value of -0.23, which sharply decreases in the elec-TS (-0.45). Then, once passed the elec-TS, the covariances between these basins begin to increase reaching a value of -0.37 in the Keto form. On the other hand, after excitation, the electrons belonging to the basins $V(O2)$ and $V(C,O)$ quite fluctuate with each other, with a covariance of -0.44 in the FC, than then increases with the course of the reaction reaching a value of -0.34 in the Keto. This implies that these basins are more correlated in the FC that in the Keto structure.

The covariances between the $V(O2)$ and the $V(O,H)$ basins have a value of -0.27 in the Enol form of $S0$. Then, after the rupture of the $O-H$ bond, the $V(O1)$ basin arises, whose electrons fluctuate with the $V(O2)$ with a covariance of -0.49 in the elec-TS. Then, from the elec-TS to the Keto form, the covariances between these basins slowly decreases, reaching a value of -0.53. This implies that the electrons belonging to these basins are more correlated after proton transfer, i.e., in the Keto structure of $S0$. In the ESIPT process, the covariances between these basins remain practically constant, having a value of -0.52 in the FC that slightly increases to -0.48 in the elec-TS. In the Keto, the covariance is again the same as in the Enol.

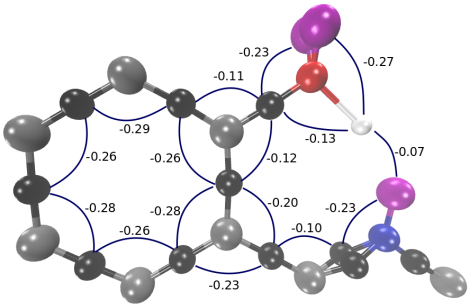

Figure 4.28: Covariances in the Enol structure of $S0$.

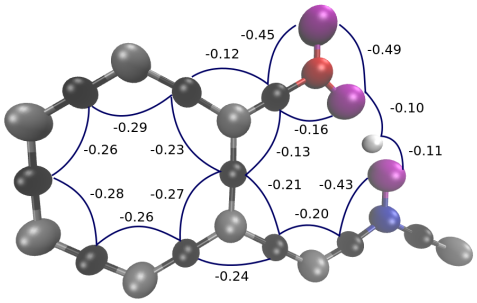

Figure 4.29: Covariances in the elec-TS of S0.

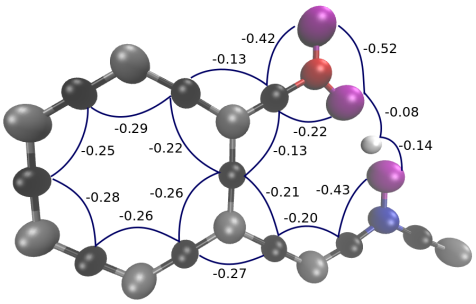

Figure 4.30: Covariances in the TS of $S0$.

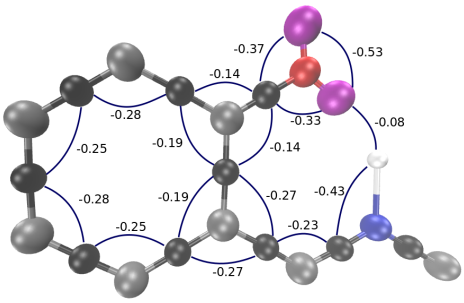

Figure 4.31: Covariances in the Keto structure of $S0$

.

From fluctuations between the basins adjacent to the nitrogen, we can see that the electrons of to the basins $V(C7,N)$ and $V(N)$ fluctuate with a covariance of -0.23 in the Enol of $S0$, which decreases enormously in the elec-TS to -0.43, to then keep constant until the end of the reaction. The electronic fluctuation between these basins also increases after the excitation, changing from -0.23 to -0.45 in the FC, to later slightly increase in the elec-TS

(-0.43) (the same value that in the elec-TS of $S0$). Then, before the appearance of the symmetrical attractors corresponding to the $V(N)$ basins located on both sides of the nitrogen atom, the covariance between the basins $V(C7, N)$ and $V(N)$ remains constant. After this bonding catastrophe, the electrons are less delocalized among the $V(N, H)$, the $V(N)$ and the $V(C7, N)$, implying a decreasing in the fluctuations, and thus, and increasing in the covariances. On the other hand, the covariances between the basins $V(C3, C7)$ and $V(C7, N)$ have the small value -0.10 in the Enol structure of $S0$. This small fluctuation increases in the elec-TS, to -0.20. Then it keeps constant until the Keto of $S0$. Also, it is possible to observe a very similar behavior through the excitation. In fact, going from the Enol to the FC structure, the covariances reaches a value of -0.22, increasing slightly to -0.20 as in the elec-TS structure of $S0$.

Finally, it is possible to observe that the covariances in the FC structure are, in general, more negative than the covariances in the Enol and also, the covariances in the elec-TS of $S0$ are qualitatively similar to the ones of the FC. Thus, the excitation process entails an activation of the molecule due to an increase of the electronic delocalization among the basins contiguous to the reaction site.

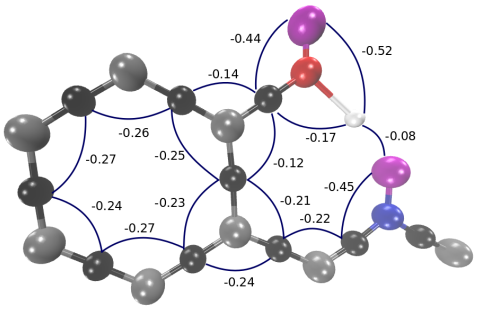

Figure 4.32: Covariances in the FC structure of $S1$.

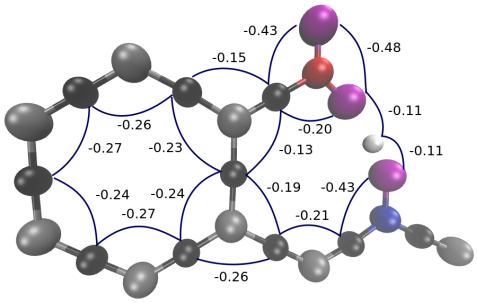

Figure 4.33: Covariances in the elec-TS of $S1$.

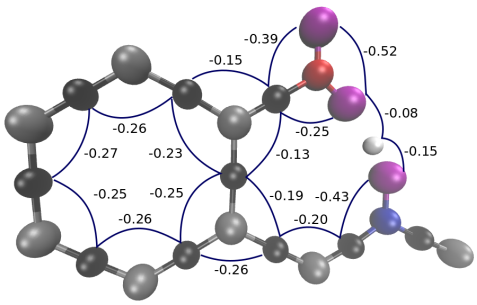

Figure 4.34: Convariances at $r_{OH} = 1.28$Å in $S1$.

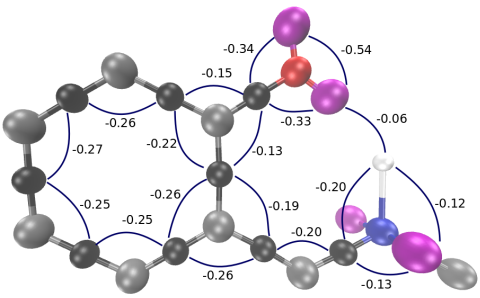

Figure 4.35: Covariances in the Keto structure of $S1$.

Core-valence bifurcation index

In section 2.2.1 we introduce the core-valence bifurcation index, and we show how, by means of this index, to classify the H-bond interaction according to if it corresponds to a purely classical (Coulombical) interaction or if there is an electronic delocalization between the donor group and the acceptor atom. In the SMA molecule, in its Enol form, there is an H-bond between the hydrogen atom in the hydroxyl group ($O-H$) and the nitrogen, while in the Keto form, the H-bond is between the hydrogen in the $N-H$ bond and the oxygen atom. Thus, the core-valence bifurcation index allows an understanding of the variation of the strength of the H-bond between the Enol and Keto structures, and also, after an excitation process.

Structure	$\eta(C(O), V(OH))$	$\eta\,(V(OH), V(N))$	$\nu\,(OHN)$
Enol	0.109	0.203	-0.094
FC	0.116	0.231	-0.115

Table 4.1: Core-valence bifurcation index in the Enol for both $S0$ and $S1$ states.

The values of the bifurcation points between the basins involved in the H-bond in the Enol structure for both $S0$ and $S1$ states are shown in the table 4.1. In this, it is evident that the H-bond it gets stronger after a vertical excitation, favoring the proton transfer in the excited state. Moreover, the more negative value for ν implies that this intramolecular interaction has a more covalent character in $S1$ than in $S0$, which is directly related with the fact that there is a higher electronic fluctuation between the basins $V(OH)$ and $V(N)$ in the excited state.

Structure	$\eta(C(N), V(NH))$	$\eta\,(V(NH), V(O))$	$\nu\,(OHN)$
Keto $S0$	0.101	0.179	-0.078
Keto $S1$	0.101	0.138	-0.115

Table 4.2: Core-valence bifurcation index in the Keto for both $S0$ and $S1$ states.

On the other hand, from the values depicted in the table 4.2, we can see that the H-bond in the Keto structure is more covalent in the ground state than in the excited state, which would favor the inverse proton transfer over the direct process.

4.4.1 *Covariance* index

Although that the spreading index σ gives us insights about the loss of aromaticity of the molecule along the proton transfer, this does not allow us to compare the loss of aromaticity between the process in both electronic states. A better description of this phenomenon is given in terms of the covariances between the basins $V(C_i, C_j)$ of the aromatic ring. In this description we consider the fluctuations between basins not only to first neighbors but to second and third as well. Thus, we defines a *covariance index* δ, which corresponds to the

negative of the total stardard deviation σ^2 in the aromatic ring [6], and is given by

$$\delta = \frac{1}{2}\sum_{a=1}^{N}\sum_{b=1}^{N}\langle cov\left(\Omega_a, \Omega_b\right)\rangle = \delta^{(1)} + \delta^{(2)} + \delta^{(3)}, \tag{4.4}$$

where the Ω_a are any of the disynaptic basins of the aromatic ring, $\delta^{(1)}$ the covariance of first neighbors, $\delta^{(2)}$ the covariance of second neighbors and $\delta^{(3)}$ the covariance of third neighbors. Then, the loss of aromaticiy is simple given by the difference of the covariance index between the Keto and the Enol isomers, i.e.,

$$\Delta\delta = \delta_{Keto} - \delta_{Enol}. \tag{4.5}$$

The fluctuations between the attractors included in δ are depicted in the Figure 4.36: blue lines indicates fluctuations to first neighbors, red dashed line represent fluctuations to second neighbors and green dashed line represents fluctuations to third neighbors.

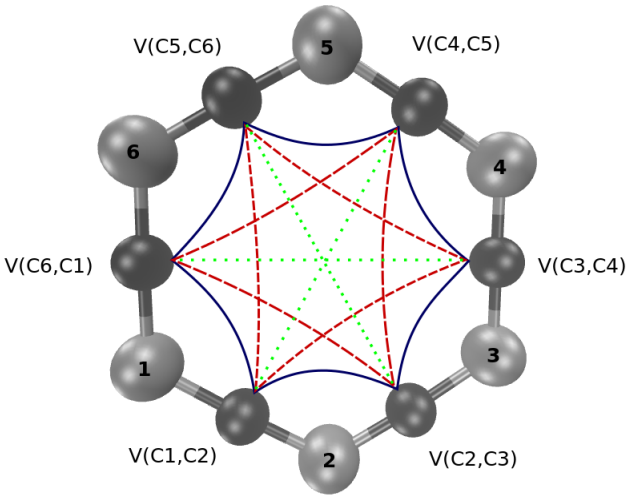

Figure 4.36: Covariances between $V(C_i, C_j)$ basins in the aromatic ring to first, second and third neighbors.

Basins	$V(C_1, C_2)$	$V(C_2, C_3)$	$V(C_3, C_4)$	$V(C_4, C_5)$	$V(C_5, C_6)$
$V(C_1, C_2)$					
$V(C_2, C_3)$	-0.26				
$V(C_3, C_4)$	-0.03	-0.28			
$V(C_4, C_5)$	-0.02	-0.03	-0.26		
$V(C_5, C_6)$	-0.03	-0.02	-0.03	-0.29	
$V(C_6, C_1)$	-0.28	-0.03	-0.02	-0.03	-0.26

Table 4.3: Covariances in the Enol form of $S0$.

Basins	$V(C_1, C_2)$	$V(C_2, C_3)$	$V(C_3, C_4)$	$V(C_4, C_5)$	$V(C_5, C_6)$
$V(C_1, C_2)$					
$V(C_2, C_3)$	-0.25				
$V(C_3, C_4)$	-0.02	-0.19			
$V(C_4, C_5)$	-0.02	-0.02	-0.19		
$V(C_5, C_6)$	-0.04	-0.01	-0.03	-0.28	
$V(C_6, C_1)$	-0.28	-0.02	-0.01	-0.02	-0.25

Table 4.4: Covariances in the Keto form of $S0$.

Values of covariances between the basins in the Enol and Keto form of $S0$ are shown in Tables 4.3 and 4.4, respectively. From this data we obtain the values of $\delta_{Enol}^{(S_0)} = -1.87$ and $\delta_{Keto}^{(S_0)} = -1.63$ for the covariances index in the Enol and Keto structures, respectively. Hence, the difference between these values gives us a value of 0.24, which represents a loss of aromaticity due to the fact that the covariance index in the Keto form is less negative.

Basins	$V(C_1, C_2)$	$V(C_2, C_3)$	$V(C_3, C_4)$	$V(C_4, C_5)$	$V(C_5, C_6)$
$V(C_1, C_2)$					
$V(C_2, C_3)$	-0.27				
$V(C_3, C_4)$	-0.02	-0.23			
$V(C_4, C_5)$	0.00	-0.02	-0.25		
$V(C_5, C_6)$	-0.02	-0.01	-0.02	-0.26	
$V(C_6, C_1)$	-0.24	-0.02	-0.01	-0.02	-0.27

Table 4.5: Covariances in the FC.

Basins	$V(C_1, C_2)$	$V(C_2, C_3)$	$V(C_3, C_4)$	$V(C_4, C_5)$	$V(C_5, C_6)$
$V(C_1, C_2)$					
$V(C_2, C_3)$	-0.25				
$V(C_3, C_4)$	-0.02	-0.25			
$V(C_4, C_5)$	-0.01	-0.03	-0.22		
$V(C_5, C_6)$	-0.02	-0.01	-0.02	-0.26	
$V(C_6, C_1)$	-0.25	-0.03	-0.01	-0.03	-0.27

Table 4.6: Covariances in the Keto form of $S1$.

The covariances in the aromatic ring of the FC and the Keto structure of $S1$ are shown in Tables 4.5 and 4.6, respectively. The covariance index in the FC is of $\delta_{FC}^{(S_1)} = -1.66$, which accounts for a reduction of the electronic delocalization in the aromatic ring after excitation, which is in agreement with the increase of the electronic delocalization in the functional groups. The covariance index after the ESIPT is of $\delta_{Keto}^{(S_1)} = -1.68$, which is slightly lower than the value in the FC. Hence, the difference of -0.02 between the Keto and the FC indicates that there is no loss of aromaticity in the ESIPT, but only a spreading of the electronic population in the aromatic ring. Therefore, in the absence of loss of aromaticity in the ESIPT process, we can conclude that there is no decrease of stability in the molecule, contrary to what happens in the ground state proton transfer, favoring the photochemical process above the purely thermodynamic one.

Chapter 5

Conclusions

5.1 About GSIPT

- In the intermediate region of the ground state proton transfer, located between 1.12Å and 1.40Å, there is a monosynaptic basin associated to the hydrogen atom: this is the principal evidence that this simple process occurs via this independent entity, and that, the rupture of the $O-H$ bond and the formation of the $N-H$ are not simultaneous.
- The rupture of the $O-H$ bond occurs several points before the TS. From a chemical point of view, this fact indicates that the electronic processes involved in a chemical reaction occur before the thermodynamical transition state (located at 1.28Å).
- The proton transfer process does not correspond to a transference of a bare proton, but a partially screened proton.
- In the valence structure of the oxygen atom in the Keto form, there is an electronic population of 5.59, which is quite high compared with the electronic population of an oxygen atom in a Lewis structure predicted by the organic chemistry. The associated electrostatic repulsion is in our opinion the main source of a barrier for the proton transfer.
- There is a spreading of the electronic population of the bonds in the aromatic ring, which is related to a loss of aromaticity after the proton transfer process.
- We define a covariance index that allows quantifying the loss of aromaticity of the ring along the reaction. This index indicates that there is a loss of aromaticity along the path of ground state proton transfer.
- There is an electronic flux from the aromatic ring to the functional groups along proton transfer.
- There is a point located at $r_{OH} = 1.20$Å at which the covariances between the basin associated to the proton, $V(H)$, and the basin of the donor atom, $V(O)$, is the same that the covariances between $V(H)$ and the basin associated to the acceptor atom $V(N)$. This means that, at this point, electrons belonging to $V(H)$ are as correlated with $V(O)$ as with $V(N)$. We called this point *electronic transition state*.

5.2 About ESIPT

- The excitation energy of the Enol form is 3.94eV, which is a good prediction of the TD-DFT, considering that the experimental value is 3.97eV.
- We have defined, for the first time, a working expression for the electron localization function for excited states using only information of the ground state KS orbitals and transition probabilities from TD-DFT.
- The detachment of the hydrogen atom of the oxygen occurs quite early compared with the proton transfer in $S0$: while in the ground state, this catastrophe occurs at $r_{OH} = 1.12$Å, in the excited state it occurs at $r_{OH} = 1.06$Å.
- The basic character of the nitrogen atom is enhanced: its electronic population at the pseudo-FC is of 3.00, which remains practically constant until slightly before the attachment of the hydrogen to the nitrogen.
- The domain of the proton transfer in which the hydrogen atom exists as an independent entity is from $r_{OH} = 1.06$Å to $r_{OH} = 1.38$Å, which is longer than in the ground state.
- In the intermediary region of the ESIPT, the hydrogen atom, which has a positive charge of 0.65e, feels a great electrostatic attraction to the nitrogen, due to the three non-bonding electrons located in the valence of this atom.
- There is a driven force produced by the excess of charge of the nitrogen on the hydrogen atom. This is the main physical argument that would explain that the proton transfer in the excited state occurs without an energetic barrier.
- The $V(N,H)$ basin appears at $r_{OH} = 1.40$Å with an electronic population of 3.33 (in the ground state this basins appears with an electronic population of 2.66). This excess of electronic density localized in the volume of the $V(N)$ would imply that this molecular structure is a unstable one.
- At $r_{OH} = 1.54$Å, it appears two new attractors associate to the valence of the nitrogen, placed symmetrically to both sides of the molecular plane. Thus, there are 1.21 electrons in excess over the nitrogen, which gives it a radical character.
- The elec-TS is located at $r_{OH} = 1.16$Å.
- The covariances in the FC structure are, in general, more negative than the covariances in the Enol form, and also, behave similarly to the covariances in the elec-TS in $S0$. Thus, the excitation process entails an activation of the molecule due to an increase of the electronic delocalization among the basins contiguous to the reaction site.
- The covariance index in the FC is of -1.66, which accounts for a reduction of the electronic delocalization in the aromatic ring after excitation, which is in agreement with the increase of the electronic delocalization in the functional groups. The covariance index after ESIPT is -1.68. Therefore, there is no loss of aromaticity in the ESIPT, but only a spreading of the electronic population in the aromatic ring.
- There is not lost of stability associated to changes of aromaticity (electron delocalization along the ring) in the molecule, contrary to what happens in the GSIPT, favoring the photochemical process above the purely thermodynamic one.

Bibliography

Bibliography

Electron localization function

[1] Becke A., *Hartree-Fock exchange energy of an inhomogeneous electron gas*, Int. J. Quantum Chem. , 23), 1915 (1983).

[2] Becke A., Edgecombe K., *A simple measure of electron localization in atomic and molecular systems*, J. Chem. Phys, 92, 5397 (1990).

[3] Silvi B, Savin A., *Classification of chemical bonds based on topological analysis of electron localization functions*, Nature, 371, 683 (1994).

[4] Savin A., Nesper R., Wengert S., Fassler T., *ELF: the electron localization function*, Angew. Chem, 36(17), 1808 (1997).

[5] Feixas, Ferran, et al., *Electron localization function at the correlated level: a natural orbital formulation*, J. Chem. Theory Comput., 6.9:2736-2742 (2010).

[6] Silvi B. and Ratajczak H., *Hydrogen bonding and delocalization in the ELF analysis approach*, Phys. Chem. Chem. Phys.,18, 27442-27449 (2016).

Topological analysis and bonding theory

[7] R F W Bader, T T Nguyen-Dang and Y Tal,*A topological theory of molecular structure*, Rep. Prog. Phys., Vol. 44, (1981).

[8] Krokidis X., Noury S., Silvi B., *Characterization of elementary chemical processes by catastrophe theory*, J. Phys. Chem. A, 101, 7277-7282 (1997).

[9] Krokidis X., et al., *How Malonaldehyde bonds change during proton transfer*, J. Phys. Chem. A, 102, 5065-5073 (1998).

[10] Alikhani, Fuster F., Silvi B., *What can tell the topological analysis of ELF on hydrogen bonding?*, Structural chemistry, 16, 203 (2005).

[11] Feixas F., et al., *The topological analysis of the electron localization function. A Key for*

a position space representation of chemical bonds, J. Chem. Theory Comput., 6(9), 2736 (2010).

Time-dependent density functional theory

[12] F. Aryasetiawan and O. Gunnarsson, *Exchange-correlation kernel in time-dependent density functional theory*, PRB 66, 165119 (2002).

[13] Dreuw A., Head-Gordon M., *Single-reference ab initio methods for the calculation of excited states of large molecules*, Chem. Rev., 105, 4009-4037 (2005).

[14] Casida M. E., *Time-dependent density functional theory for molecules and molecular solids*, Theochem, 914, 3-18 (2009).

[15] Chatterje K., Pernal K., *Excitation energies from extended random phase approximation employed with approximate one- and two-electron reduced density matrices*, J. Chem. Phys., 137, 204109 (2012).

[16] Chapter 7, 8 and 9 in Ullrich C., *Time-dependent density-functional theory: concepts and applications*, Oxford University Press (2012).

[17] Adamo C., Jacquemin D., *The calculations of excited-state properties with Time-Dependent Density Functional Theory*, Chem. Soc. Rev., 42, 845 (2013).

Intramolecular proton transfer

[18] Douhal A., et al.,*Proton-transfer reaction dynamics*, Chemical physics 207, 477-498 (1996).

[19] Ortiz-Sánchez JM., et al., *Theoretical study on the excited-state intramolecular proton transfer in the aromatic Schiff base Salicylidene Methylamine: an electronic structure and quantum dynamical approach*, J. Phys. Chem. A., 13;110(14):4649-56 (2006).

[20] Ortiz-Sánchez JM, et al., *Electronic and quantum dynamical insight into the ultrafast proton transfer of 1-hydroxy-2-acetonaphthone*, J. Chem. Phys., 28;127(8):084318 (2007).

[21] Ortiz-Sánchez JM. et al., *Electronic-structure and quantum dynamical study of the photochromism of the aromatic Schiff base salicylideneaniline*, J. Chem. Phys., 129.21, 214308, (2008).

[22] Kwon Ji Eon, Soo Young Park, *Advanced organic optoelectronic materials: harnessing excited-state intramolecular proton transfer (ESIPT) process*, Advanced Materials 23.32, 3615, (2011).

[23] Jankowska J., et al., *Photophysics of Schiff Bases: Theoretical Study of Salicylidene Methylamine*, Chem. Phys. Chem., 13(18) (2012).

[24] Jianzhang Zhao, Shaomin Ji, Yinghui Chen, Huimin Guo and Pei Yang, *Excited state intramolecular proton transfer (ESIPT): from principal photophysics to the development of new chromophores and applications in fluorescent molecular probes and luminescent materials*, Phys. Chem. Chem. Phys., 14, 8803–8817 (2012).

[25] Gutiérrez-Arlauz L. et al., *Ultrafast excited state hydrogen atom transfer in salicylideneaniline driven by changes in aromaticity*, Phys. Chem. Chem. Phys., 17, 31608-31612, (2015).

[26] Sporkel L. et al., *Photoswitching of salicylidene methylamine: a theoretical photodynamics study*, J. Phys. Chem. B, 119.6:2702-2710 (2014).

Quantum chemistry and density functional theory

[27] Robert G. Parr, Robert A. Donnelly, Mel Levy, and William E. Palke, *Electronegativity: The density functional viewpoint*, J. Chern. Phys. 68(8) (1978).

[28] Parr, G., Yang, W., *Density Functional Theory of atoms and molecules*, Oxford University Press (1989).

[29] Chapter 3 and 4 in Szabo A. and Ostlund N., *Modern Quantum Chemistry. Introduction to advanced electronic structure theory*, Dover Books on Chemistry (1996).

[30] John P. Perdew, Kieron Burke and Yue Wang, *Generalized gradient approximation for the exchange-correlation hole of a many-electron system*, PRB 54, 23 (1996-I).

[31] Goedecker S., Umrigar C. J., *Natural orbital functional for the many-electron problem*, PRL 81, 4, 866 (1998).

[32] Chapter 8 in Cioslowski, *Many-electron densities and reduced density matrices*, Springer Science+Business Media, LLC (2000).

[33] Chapter 5 and 6 in Jensen F., *Introduction to computational chemistry*, Wiley (2007).

[34] Á. Nagy 1 and C. Amovilli, *Electron-electron cusp condition and asymptotic behavior for the Pauli potential in pair density functional theory*, J. Chem. Phys. 128, 114115 (2008).

[35] Chapter 3 and 8 in Foresman J. and Frish A., *Exploring chemistry with electronic structure methods*, Gaussian Inc., third edition (2015).

Algebraic methods in chemical bonding

[36] Matamala A. R., *Discrete and Continuum Quantum States for the Kratzer Oscillator*, Int. J. Quantum Chem. Vol 89, 129 –134 (2002).

[37] Matamala A. R., Maldonado C. R., *A simple algebraic approach to a nonlinear quantum oscillator*, Physics Letters A 308 319–322 (2003).

[38] C. Amuba Singh, O. Babynanda Devi, *Ladder Operators for the Kratzer Oscillator and the Morse Potential*, Int. J. Quantum Chem., Vol 106, 415– 425 (2006).

[39] Mikulski D., Molski M. and Konarski J., *On an algebraic approach to the Kratzer oscillator*, Phys. Scr. 80 (2009).

[40] Maulen B., *SO(2,1) dynamical symmetry of Kratzer oscillator in diatomic molecules*, arXiv:1704.04346v2 (2017).

Miscellany

[41] Fukui K., *The path of chemical reactions-The IRC approach*, Accounts of Chemical Research, 14, 12, 363 (1981).

[42] Chapter 14 in Greiner W., Neise L., Stöcker H., *Thermodynamics and Statistical Mechanics*, Springer (1995).

[43] Chapter 2 in Fetter A. and Walecka J.D., *Quantum Theory of Many-Particle Systems*, Dover Publications Inc., United States (2003).

[44] Tempel D. G. et a., *Time-Dependent Density Functional Theory of Open Quantum Systems in the Linear-Response Regime*, J. Chem. Phys. 134, 074116 (2011).

[45] Chapter 3 in Sauer S., *Molecular electromagnetism. A computational chemistry approach*, Oxford Graduate Texts (2011).

[46] Pittalis S. et al., *Ab initio theory of spin entanglement in atoms and molecules*, PRB 91, 075109 (2015).